CoA/M/Mat - 42

CoA. Memo. Mat. 42

ST. NO.
U.D.C. 30546
AUTH.

THE COLLEGE OF AERONAUTICS

CRANFIELD

PRELIMINARY REPORT ON AN INVESTIGATION INTO THE BEHAVIOUR OF THE ALUMINIUM ALLOY RR58 UNDER COMBINED CREEP AND FATIGUE CONDITIONS

COLLEGE OF AERONAUTICS LIBRARY

A. YOUNGER, T.E. CLIFTON and R.G.C. HILL

30546

3 8006 10039 1443

THE BEHAVIOUR OF THE ALUMINIUM ALLOY RR58 UNDER COMBINED CREEP AND FATIGUE CONDITIONS

Part I: The hydraulic combined creep and fatigue machine

A. Younger, B.Sc., Ph.D., A.I.M.

and

T.E. Clifton, Grad.I.Mech.E.

COLLEGE OF AERONAUTICS LIBRARY

PRELIMINARY REPORT ON AN INVESTIGATION INTO THE BEHAVIOUR OF THE ALUMINIUM ALLOY RR58 UNDER COMBINED CREEP AND FATIGUE CONDITIONS

INDEX

The hydraulic combined creep and fatigue machine

The experimental rig was designed to fulfil three major functions, namely:-

(a) The application of a static tensile load and the measurement of the strain time relationship.

(b) The superimposition of a varying dynamic stress of a given amplitude on the static stress. This dynamic stress was to act in the same direction as the static stress.

(c) The measurement of strain recovery under a reduced static stress, with and without the superimposition of a dynamic stress.

In order that the tests could be carried out under precise experimental conditions the following design requirements were postulated:-

(a) The load must at all times be applied axially with no bending moments. The load will be maintained constant at the desired value irrespective of creep strain. The mechanism for applying the load and for its measurement shall be essentially free from frictional effects.

(b) The static loading system shall be of low inertia. This condition is necessary in view of the dynamic stressing and precludes any form of dead-weight loading.

(c) The maximum combination of static and dynamic loads shall be not less than 0.6 tons.

(d) The frequency of the dynamic load shall be variable from 0 to 50 cycles per second, and the maximum amplitude of this load shall be 20% of the total maximum combined load.

(e) The strain produced in the specimen shall be continuously recorded and there will be continuous monitoring of both the static and dynamic loads.

(f) There will be provision for elevated temperature testing up to 200°C, the specimen gauge length being maintained at $\pm$ 1°C of a prescribed temperature.

Consideration of these requirements, particularly the need for high actual loads coupled with rapid response times led to the adoption of an hydraulic system of loading. Axial load is applied to one end of the specimen by a double-acting hydraulic jack; the other end of the specimen being rigidly linked to a steel beam simply supported on rollers. The output from strain gauges attached to this beam is used as the controlling feed-back to a servo valve controlling the hydraulic flow to the jack. Externally generated D.C. and A.C. signals position this valve for the required static and dynamic load displacements respectively.

A general view of the whole apparatus including the measuring and control equipment is shown in Figure 1. The detailed construction of the apparatus can be seen in the exploded drawing in Figure 2. All components subject to load were machined from high tensile steel and the hydraulic system was designed to withstand internal pressures of 3000 p.s.i.

For simplicity the apparatus is described under four functional headings, i.e., mechanical construction, load control, strain measurement, and temperature control.

1.1 Mechanical construction

The hydraulic jack consists of a steel block containing a sliding piston, the parts being arranged to allow oil flow to each side of the piston. The piston and its connecting rods are machined from high tensile steel, the outside piston being 1.875 ins. with an effective annular pressure area on both faces of 1.75 sq. ins. At the normal operating pressure of 1500 p.s.i., a theoretical maximum load of 1.2 tons can be applied, but this figure is considerably reduced by the back pressure on the other piston face. Neoprene 'O' ring seals on the piston assembly allow movement of the piston whilst still providing an hydraulic seal. The maximum piston movement is $\pm$ 0.15 ins. about its centre position. One end of the piston is rigidly connected to the specimen, whilst the other end of the piston protrudes from the body of the jack and operates a cut-out switch for the hydraulic pump, if the maximum permissible piston movement is reached during a test.

The body and end-caps of the jack are machined from mild steel with all the internal and mating faces ground. One side and the base of the jack were precision machined for the attachment of the control valve and for clamping to the base-plate respectively. An adaptor plate machined from a light alloy connects the servo valve outlets to the inlet ports of the jack. Sealing on both sides of this adaptor plate is by suitable neoprene 'O' rings.

The jack assembly is rigidly bolted to a 1" thick ground mild steel base plate. Also bolted to this plate is the housing containing the load measuring beam and the second specimen grip. Tie bars on their upper surfaces also link the jack and the beam housing and prevent bending of the whole assembly during high specimen loadings. The base plate is firmly mounted in a mild steel angle frame and surrounded by an oil spillage tray.

During early development of this rig the steel measuring beam was rigidly clamped to the rear of the beam housing. Under high loads some slip occurred between the beam and the clamps resulting in sudden alterations in the applied load. This slip was not reversed on unloading and so produced increasing zero errors in the load measurements. This problem was overcome by redesigning the beam to bear on hardened rollers (see exploded view Figure 2). Two pairs of rollers, one on each side of the beam at both ends are held in position by two spring loaded plates. Horizontal and vertical shifts in the beam position are prevented by dowel rods surrounding the beam. Thus the only permitted movement of the beam is a free deflection upon a force being applied at its centre by the rigidly attached specimen grip. The whole of this beam housing is rigidly fixed to a steel block through which the specimen grip passes. Considerable attention was given to the alignment of the beam housing with respect to the piston movement in order that true axial loading can be applied. The position and attachment of the strain gauges on the measuring beam is described in a later section.

1.2 Hydraulic system and load control

A block diagram of the hydraulic system is shown in Figure 3. Oil at controlled pressure from an hydraulic power-pack (Keelavite Type No. 23442) is passed through a filter, a precision reducing valve and a second micro-filter before being admitted to the servo control valve. Pressure is gauged both at the outlet of the pump and the inlet to the servo valve and an accummulator placed after the reducing valve helps to smooth out fluctuations in pressure. Two stage filtration has been found to be essential as the servo valve is extremely sensitive to any foreign particles in the oil. The oil used is Shell Tellus Number 27. So far it has not been found necessary to introduce any cooling for the oil.

The servo valve used throughout these tests has been a Dowty Moog Series 21 flow control valve. This consists of a polarized electric-force motor with two stages of hydraulic amplification. The motor armature passes through a tubular flexure pivot which also acts as the seal between the electromagnetic and the hydraulic parts of the valve. At the end opposite to the motor, the armature passes between two nozzles creating variable orifices between the nozzle tips and the armature. Pressure oil is supplied to these orifices through

two fixed upstream orifices and the intermediate chamber pressures are vented to either end of the output stage spool. The spool is of conventional four-way design and is spring centred. Output flow from the valve, at a fixed valve pressure drop is proportional to spool displacement. When a signal is applied to the motor the armature moves between the two nozzles opening one and closing the other resulting in a pressure differential between the nozzle chambers. This pressure differential acts on the second stage spool, resulting in displacement and hence output flow proportional to electrical input signal. The motor coil is wound for differential current input thus allowing signals of either polarity to be used.

The valve is driven by a transistorized D.C. servo-amplifier with a sensitivity of 1mV for full rated output and an input impedance of 4.5 KΩ. The output of the amplifier is operated in push-pull. A D.C. signal derived from a potential divider across a dry cell (the 'static' component of load) is fed into the servo-amplifier together with an A.C. signal derived from a standard oscillator (the dynamic component of the load). The feed-back loop is completed with the output signal obtained from the strain gauges attached to the load measu rement beam (Figure 4).

The semi-conductor strain gauges, manufactured by Ether-Langham Thompson, were attached to the load measuring beam by a thermosetting 'Araldite' resin adhesive and connected in a four active arm bridge network. An 'Apex' potentiometer was used for initial bridge balancing. A stable transistorized voltage source supplies a constant potential of 4V to the bridge, which keeps the gauge current below the safe continuous working value. By the use of semi-conductor type strain gauges a voltage output is obtained which is sufficient in amplitude to make further amplification unnecessary. Previously standard wire gauges were used which did require considerable amplification in order to obtain a signal large enough to feed the servo amplifier. This system had two main disadvantages. Firstly the use of amplification introduced self-errors. Secondly when using an alternating (fatigue) load the A.C. feed back signal became seriously out of phase with the applied A.C. signal. This produced a distorted load-time waveform. When using the semi-conductors gauges the waveform closely approximates to the sinusoidal.

It is found, in practice, that outputs of approximately 250mV are produced directly by the bridge network at the normal maximum load. This output is sufficient to allow load constancy of $\pm \frac{1}{2}\%$ to be maintained. The bridge output is continuously monitored on a digital voltmeter (Blackburn Type 2114) at a reading frequency of 3 per second. This enables both the static and dynamic components to be measured.

An oscilloscope is used to monitor the dynamic load and to study its waveform. The precise amplitude of the wave can be measured by taking the maximum and minimum readings of the digital voltmeter over a short period of time. The mean of these readings is the static component of the load.

1.3 Strain measurement

The strain is measured by taking the difference in output of two identical transducers their movement being operated by the movement of the two specimen grip extension rods. These rods are of solid construction and do not creep under load. The use of two transducers is necessary because

(a) The tests are being carried out at temperatures above the maximum permitted operating temperatures of the transducers. This precludes fixing a single unit alongside the specimen.

(b) The machine is essentially a soft machine with a considerable beam deflection. It has been found that to subtract this beam movement electronically is more acceptable than to read a dial gauge and correct all the readings. Dial gauges are mounted on the framework to measure both beam movement and piston movement and thus provide a check on the transducer readings.

The transducers are of the inductive displacement type and are mounted with their bodies rigidly fixed to the jack and the beam housing respectively and their plungers moved by rigid arms attached to the specimen grip extensions. The transducer measuring bridges are operated on the conventional carrier wave system with a demodulated output proportional to measured movement. The difference output from the two units, the net specimen strain, is recorded onto a Graphispot galvanometer recorder. A component is included in the differencing circuit to ensure that the output from each transducer system for any given displacement is identical. The scale of the recorder normally provides a pen movement of 1mm per 0.0001 inch extension of the specimen, although both this scale and the chart speed can be varied.

1.4 Temperature control

A split furnace wound to give a single zone element fits around the specimen grip extension enclosing the grips and the specimen. The arrangement with one half of the furnace removed can be seen in Figure 5. A Chromel-Alumel thermocouple placed in the furnace chamber is used to control the temperature via a proportioning controller recorder. A separate thermocouple fixed near the specimen - or spot welded on to it, provides an independent check on the

EGE OF AERONA
IBRARY

temperature. Control to within $\pm$ 1°C is effected over the specimen gauge length.

Some trouble was experienced when the heat dissipated from the furnace caused non-uniform expansions in the base-plate and the tie-rods. This has been overcome by placing water-cooled plates between the furnace and the base-plate and along the tie-bars.

A steady specimen temperature is reached after a one-hour heating period and a further one-hour soaking is given before testing.

1.5 Calibration

The load beam is calibrated by replacing the specimen by a strain gauged load cell, this cell having immediately previously been calibrated in an approved tensile testing machine. Loads are applied to the load cell exactly as under the testing conditions and the load beam output recorded against the load cell output. The load beam calibration is checked at frequent intervals, although as yet little change has been detected.

The strain measurement system is calibrated in a conventional manner using a barrel-type micrometer head fixed in a jig.

1.6 Recommendations for future designs

The apparatus as described here fulfils the conditions stated at the beginning of this section. It is, however, an apparatus which has undergone many modifications and alterations during its development stage. As a consequence some further modifications to improve the general layout, the case of maintenance and the overall long term reliability would be incorporated in any new machine based on this design. The recommended modifications are that:-

(a) The axis of the machine be arranged vertically, with the jack assembly at the upper end. The jack assembly would be carried on ground steel pillars fixed to a massive base and would be adjustable in height on these pillars. The apparatus would then be able to accommodate specimens of different lengths. Sufficient width should be allowed between the pillars for the provision of a larger multi-zone split furnace, with its hinge vertical. This would greatly improve access to the specimen and allow space for the mounting and adjustment of extensometers. The necessity for cooling tie-bars, etc., would be removed. At the same time the provision of a controlled temperature enclosure around the load-beam should be considered.

(b) A single console type control cabinet should be constructed. All electronic control and measuring equipment could be housed in one section with the hydraulic controls in another. With the control units built into such a console only those controls essential to the operation of the equipment need be displayed which would considerably simplify the use of the equipment. All connections to and from the console would be screened and permanently soldered.

(c) The strain measurement system should be replaced by a single transducer mounted close to the specimen. This modification would eliminate the need for balancing two transducers. In a larger furnace a transducer could be mounted in a water-cooled jacket inside the furnace.

(d) Greater attention should be paid to the cleanliness of the hydraulic oil. Additional filters should be provided together with some arrangement for processing the oil after every refill. A larger pressure accumulator would help to maintain a more constant line pressure.

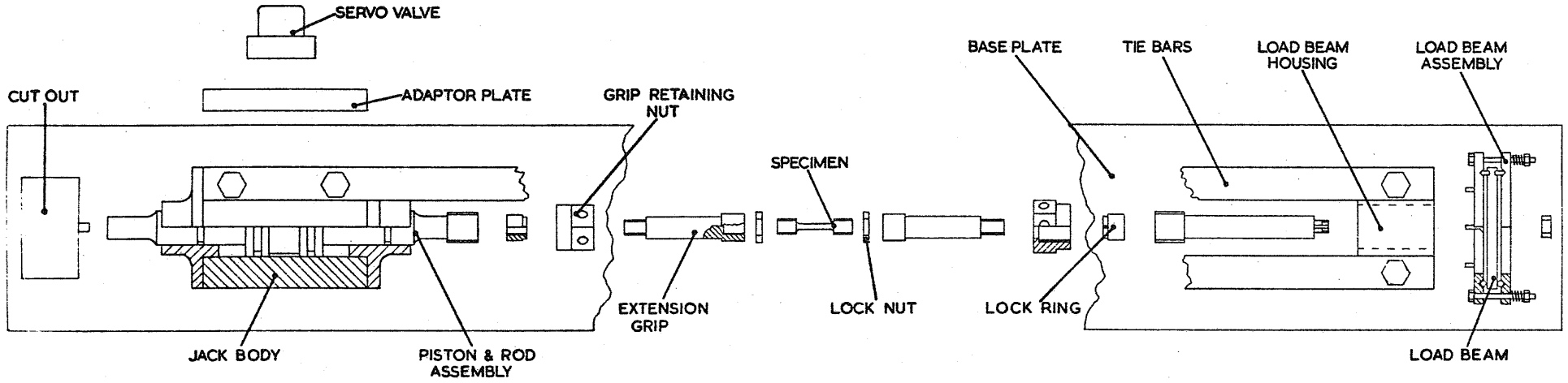

FIGURE 2 EXPLODED DRAWING OF MECHANICAL CONSTRUCTION

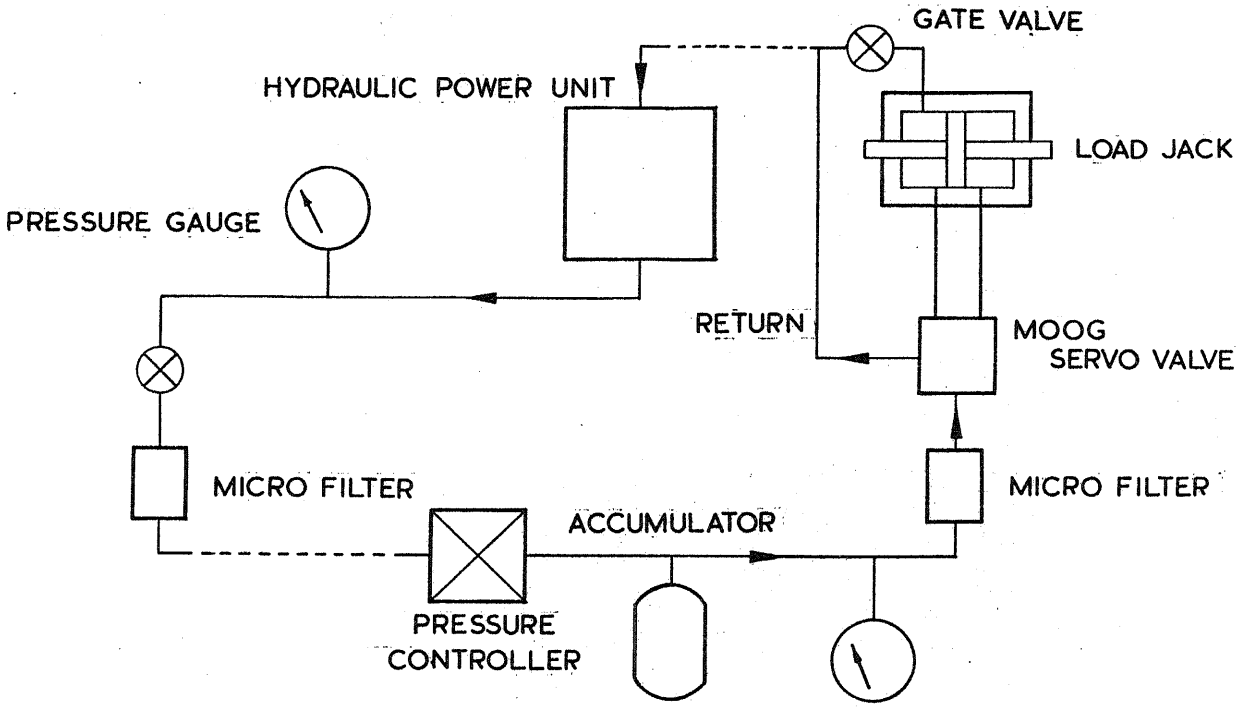

FIGURE 3 BLOCK DIAGRAM OF HYDRAULIC SYSTEM

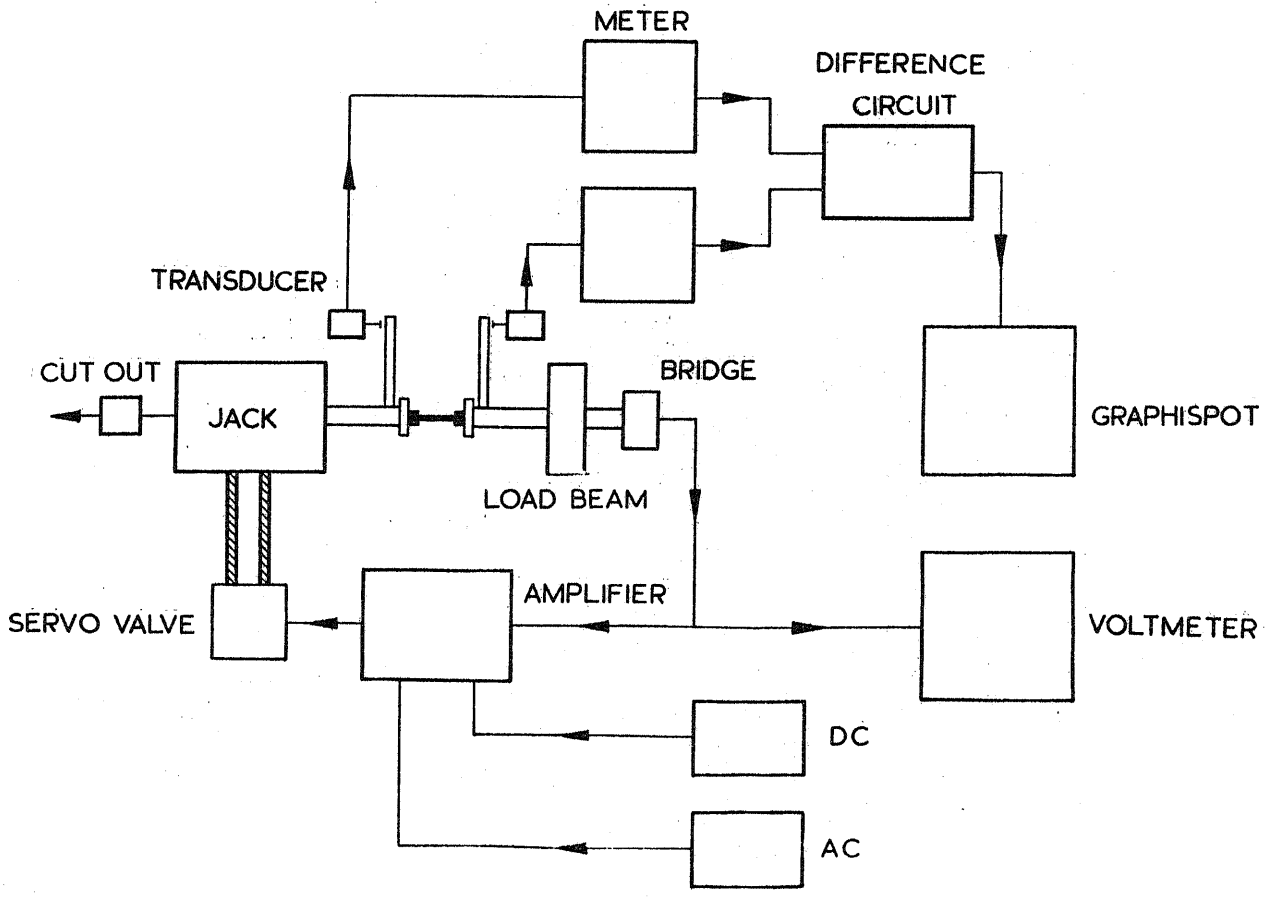

FIGURE 4 BLOCK DIAGRAM OF ELECTRICAL CONTROL SYSTEM

Part II: The initial experimental programme on the R. RR58 alloy. Combined creep and fatigue tests using the hydraulic testing machine

A. Younger, B.Sc., Ph.D., A.I.M.

and

R.G.C. Hill, B.A., B.Sc.

COLLEGE OF AERONAUTICS LIBRARY

2.1 Material and specimens

The alloy selected for the work (RR58) is of concern as it is to be used for the structure of the Anglo-French transport aircraft (Concord). RR58 has the following nominal composition:-

2.2% Copper
1.5% Magnesium
1.0% Iron
1.2% Nickel
0.1% Titanium
Remainder Aluminium

The material was received as extruded rods 0.500 ins. diameter and was heat-treated in rod form as follows:

Solution treated for 4 hours at 530°C.
Air-cooled for 10 seconds.
Quenched into cold water.
Aged for 20 hours at 190°C.

Specimens were machined from the heat-treated rods to the dimensions shown in Figure 6.

2.2 Experimental procedures

The object of this investigation is to assess the effect on the creep rate of superimposing a fatigue loading on the static creep load. In order to be able to predict possible combinations of fatigue and creep loading where changes in creep rate are significant, two multi-loading condition procedures have been followed. Although these procedures have severe limitations, they do enable a large number of load combinations to be assessed rapidly. The techniques are:-

(a) Constant static load, increasing fatigue load

A constant static load is applied to the specimen which is then also subjected to a fatigue load. The strain-time relationship is continuously recorded. After given intervals of time, the fatigue amplitudes are increased, the change usually producing some alteration in creep rate. The elongation-time curve produced by these tests is diagrammatically shown in Figure 7. The symbols used on this figure are:-

m	creep rate
F	fatigue load
L	static load
Suffix c	constant condition

This nomenclature is used on all tables relating to these curves.

(b) Constant fatigue load, increasing static load

Whilst maintaining a constant superimposed fatigue load, the basic static load is increased by uniform increments at given equal intervals. The increment in load produces an instantaneous extension (ε) containing both plastic and elastic components and is usually followed by a period of decreasing creep rate until steady state creep is obtained. This procedure is diagrammatically represented in Figure 8, the symbols used being the same as in Figure 7 with the addition of the instantaneous extension (ε). This nomenclature is used on all relevant tables.

Throughout the experiments described in this section the initial value of the static load (L_1) has been 16 t.s.i., and the time intervals 20 minutes. Although 20 minutes is insufficient under some conditions for a steady creep rate to be obtained, the last 10 minutes of this time usually gives an elongation-time curve which is approximately linear. It is the gradient of this line, over the last half of each interval, which is quoted as the creep rate.

2.3 Results for constant static load with increasing fatigue loads

The results for this series of tests at room temperature and 130°C are given in Tables I and II respectively.

(a) Tests at room temperature

There are no general patterns of increasing creep rates with either increasing static or increasing fatigue loads. At the fatigue level of $\pm$ 2.5 t.s.i., there are increasing creep rates with increased static loads, but at lower fatigue amplitudes this trend is not observed. A feature of the results at 24 t.s.i. static load is that creep recovery occurs under fatigue conditions.

(b) Tests at 130°C

Increasing fatigue amplitudes and increasing static loads both produce increasing creep rates.

2.4 Results for constant fatigue loads with increasing static loads

Tests were carried out at four constant fatigue amplitudes ($\pm$ 0.1, $\pm$ 0.5, $\pm$ 1.5, $\pm$ 2.5 t.s.i.) with the static loads being increased in 2 t.s.i. increments from 16 t.s.i. to 26 t.s.i., at a range of 8 temperatures (20°, 50°, 75°, 105°, 120°, 130°, 140° and 155°C). At the higher fatigue levels and temperatures it was not possible to complete all the static stages. The results for the instantaneous extensions and the creep rates are given in Tables III to XVIII.

(a) Tests at room temperature (Tables III and IV)

The instantaneous extensions, produced by the same increment in load, increase with the total static load and the fatigue load. There is very little creep at this temperature.

(b) Tests at 50°C (Tables V and VI)

The instantaneous extensions produced by the same load increment increase with the total value of the load and with increasing fatigue. Except at 26 t.s.i., static stress for all fatigue levels, and above 20 t.s.i. static at $\pm$ 2.5 t.s.i. fatigue, there is very little creep at this temperature.

(c) Tests at 75°C (Tables VII and VIII)

The instantaneous extensions produced by the same load increment generally increase with increasing total static load and increasing fatigue load. Both creep and creep recovery appear to occur at this temperature, the former above 20 t.s.i. static stress, the latter below this stress. The creep rate increases with increasing fatigue.

(d) Tests at 105°C (Tables IX and X)

The instantaneous extensions produced by the same load increment increase with increasing static level. Increasing the fatigue level from $\pm$ 1.5 t.s.i. to $\pm$ 2.5 t.s.i. increases the extension for all static levels. Below $\pm$ 1.5 t.s.i. differences in fatigue level appear to have little effect. Increasing the static load level for a constant fatigue level increases the creep rate. At the higher static loads increasing fatigue level gives increasing creep rates. Some creep recovery occurred at the lower fatigue levels.

(e) Tests at 120°C (Tables XI and XII)

The instantaneous extensions produced by the same load increment increase with both increasing static and fatigue levels. Above 20 t.s.i., static load, the creep rate also increases with increasing static and fatigue loads.

(f) Tests at 130°C (Tables XIII and XIV)

At the higher static and fatigue loads the instantaneous extension produced by the same load increment increases with increasing static and fatigue loads. Below 22 t.s.i. static, and ± 2.5 t.s.i. fatigue, there is little variation in the extensions produced. Creep rates increase with increasing static and fatigue loads, but little occurs below 20 t.s.i. static, except at the lowest fatigue level.

(g) Tests at 140°C (Tables XV and XVI)

The instantaneous extensions produced by the same load increment increase generally with increasing static and fatigue loads. The creep rates are low with little creep occurring below 20 t.s.i.

(h) Tests at 155°C (Tables XVII and XVIII)

Except for the lowest static values the instantaneous extensions produced by the same load increments increase with increasing static and fatigue loads. Also excepting the lowest static load (16 t.s.i.) and at ± 0.5 t.s.i. fatigue, the creep rates increase with increasing static and fatigue loads.

The creep rates quoted in Tables III to XVIII have been plotted against the reciprocal of the absolute temperature, these curves being shown in Figures 9 to 12.

2.5 Discussion

Throughout the discussion of these results one major point must be borne in mind: it is that all the values of instantaneous extension and creep rate are influenced by the prehistory of the material. This prehistory includes the heat treatment of the metal and the structural changes brought about by the test itself up to the point of measurement. For unequivocal values of the creep rates under combined static and fatigue loading conditions, a separate test using a fresh specimen must be carried out for each possible condition. This procedure

which is currently being carried out, is laborious and will require many months to complete. It is however essential for a full understanding of the interaction of static and dynamic loads over a long period of time.

In the case of the present experiments, the amount of creep that occurs in the early stages of the test is fairly small and may, in fact, have little influence on the creep rates in subsequent stages under more severe conditions. Therefore despite this fact (and also that the creep rate as measured is not the true steady-state value - see section 2.2) it is considered that the present experiments do present a fair preliminary assessment of the effects of superimposed fatigue stresses on statically loaded specimens. Thus a full analysis of these results has been made and conclusions drawn from them. These conclusions, however, may need modification when the results of the uni-specimen tests are available.

(a) Instantaneous extensions

For the same static load increment the instantaneous extension produced increases with the absolute value of the static load and when the static load exceeds 22 t.s.i., it also increases with increasing fatigue amplitude. Increasing extensions with increasing static load level would be expected from the shape of the normal load extension curve (Figure 13). Equal increments in load ab and cd produce quite different extension wx and yz. For this material at room temperature the approximate yield stress is 22 t.s.i. and the ultimate tensile strength about 29 t.s.i.

When discussing the effect of the superimposed fatigue stress on the instantaneous extensions, the value of the total maximum stress must be considered. This stress is the sum of the static stress plus the stress at the peak of the fatigue cycle. If this factor is taken into account then a change from 20 ± 2.5 t.s.i. to 22.5 ± 2.5 t.s.i. can be compared with the change from 22 ± 0.5 t.s.i. to 24 ± 0.5 t.s.i. Such a comparison has been made in Table XIX and certain conclusions can be drawn from this.

(i) When the maximum stress does not exceed the yield stress, the amplitude of the fatigue appears to have little effect on the instantaneous extensions on increasing the load, i.e., the fatigue amplitude has no effect on the Young's Modulus.

(ii) Up to about 105°C, at static maximum stress levels above the yield stress, higher fatigue amplitudes produce greater extensions. At the higher temperatures and stress levels this pattern may reverse, though there is insufficient evidence to be definite on this point.

In interpreting these results, two important facts must be considered. Firstly the specimens subjected to the higher fatigue have been strained under a lower mean stress. Secondly the specimens subjected to the lower fatigue have been given an extra stage of loading, i.e. they have been under load for a longer time and have received a larger number of fatigue cycles. These factors would tend to produce greater hardening in the specimens subjected to the lower fatigue amplitude and consequently a decrease in the instantaneous extension. Such a difference in the hardening might be visible as a difference in dislocation density or arrangement and this possibility is being investigated using thin foil electron microscopy (see Part 3). Electron microscopy may also reveal why any reversion in behaviour should occur.

(b) Creep rates

Two general facts emerge from the creep rate figures. Firstly, for a given mean stress, the mean creep rate increases with increasing superimposed fatigue loading. Secondly, for a given peak stress the mean creep rate decreases with increasing fatigue amplitude. Several explanations can be suggested to explain these facts and are discussed below.

(i) Strain rate effect

For the same maximum stress the strain rate during the part of the cycle in which the load is increasing is greater for a greater amplitude, since the frequency is constant. As the strain rate increases, the resistance to deformation also increases, thus producing less extension. At the same mean stress, the strain rate effect would be masked by the fact that the maximum stress is greater with greater amplitude. While strain rate must play some part in the observed behaviour, it is considered unlikely to be the full explanation since the magnitude of the effect is considerably greater than would be expected from a strain rate consideration alone.

(ii) The dependence of the creep rate on the load

A diagrammatic creep rate versus load curve is shown in Figure 14. If in the first case point A is the mean stress, then, as the amplitude is increased, the maximum stress increases and the minimum stress decreases. Since the creep rate-load curve is not linear but has an increasing slope with increasing load, the increase in the maximum stress produces a greater change in rate than the decrease due to the lower minimum stress. As the times in each part of the cycle are equal, the net result would be an acceleration in rate with increasing amplitude. If in the second case point A is the peak stress, as the amplitude increases so a greater proportion of lower creep rate is included giving a decreasing creep rate with increasing amplitude.

The creep rate versus peak stress curves plotted from the results in Table X, XII, XIV, XVI and XVIII are seen in Figures 15 - 19. These, with the exception of Figure 18 at 140°C where there are no low stress values, exhibit the general form shown in Figure 14. Thus this alloy would be expected to behave as predicted above. The magnitude of these effects would be greatest in the peak stress range 20 - 24 t.s.i. where the curvature of the creep rate - load curve is greatest.

(iii) Residual cyclic strain effects

A third way of considering this problem is to resolve the strain-time relationship into two components; the creep strain developed by a continuous load equal to the minimum stress in the cycle plus an increment due to the residual strain for each fatigue cycle. If it be assumed that this residual cyclic strain can be negative as well as positive, an explanation can be offered for the 'negative creep' or creep recovery found under certain conditions.

The shape of the strain-time curve during each fatigue cycle will depend on several factors. The amount of strain produced during the loading half of the cycle will depend on the work-hardening coefficient of the material

COLLEGE OF AERONAUTICS LIBRARY

at that total strain and at the same temperature; on the amplitude, in so far as it affects the incremental work-hardening and the strain rate, and on the actual peak load. The unloading part of the curve is dependent on the strain recovery behaviour of the materials, which changes little once a steady state creep behaviour has been achieved. The frequency of the superimposed fatigue loading will affect all the variables.

Considering the experimental observations stated at the beginning of this section (see page 6) from this point of view, it can be seen that for the same peak stress the continuous minimum stress for the largest amplitude is 4.8 t.s.i. lower than that at the minimum amplitude. Such a difference in stress would, for all loads (Figures 15 - 19), produce a large change in creep rate. For the same mean stress however the difference in minimum stress between the largest and smallest amplitude is only 2.4 t.s.i. Most of these minimum stresses, and many of the mean stresses, do not exceed the static yield stress of the material. Thus as the amplitude of the cycle is increased it incorporates an increasing proportion of the plastic components of the deformation. This produces greater residual strain and a faster creep rate, so long as this effect is greater than the reduction in rate due to a lower continuous minimum stress. The structural consequences of this concept are being investigated using thin foil electron microscopy, since the larger amplitudes for the same mean stress, should show a different dislocation distribution and density.

Whilst all these explanations can satisfy the two general facts, it is considered that no one explanation is complete and that they all contribute to the overall mechanism. A variable not yet investigated is the frequency of the fatigue cycle. An increase in frequency would accelerate all the relevant strain rates and therefore should not modify the strain rate effect as such; neither should it affect the 'creep rate versus load' effect. It would however considerably modify the residual cyclic strain effect. The shape of the load-strain curve would be modified particularly at higher temperatures due to the change in strain rate and the time available for recovery would be severely curtailed. Some similar tests to those reported here are being carried out at 180 c/s and will be reported in a subsequent section of this report.

An important factor which has been ignored so far in this discussion is the role of ageing in the creep behaviour of this material. Graphs have been drawn of the creep rate versus the reciprocal of the absolute temperature under identical loading conditions (Figures 9 - 12). These show that a single thermally activated process cannot account for the observed pattern of creep behaviour over the temperature range 20 - 155°C. The activation energies derived from these curves, at least in the temperature range 100 - 130°C, are of the order of 2-3 Kcals/mole which are well below that for normal self-diffusion in aluminium. It is more in accordance with the quoted energies for dislocation-precipitate interactions. These interactions are being investigated using electron microscopy.

2.6 Future work

Experiments are currently in progress on the extension of these results to higher frequencies (160 c/s) and to higher fatigue amplitudes. Some work has also been carried out to determine the fatigue life of this material under these combined conditions. Other tests, associated with electron microscopy work have been carried out on an Instron machine to study the structural changes brought about by a low number of cycles of fatigue under creep conditions. All these experiments will shortly be reported in subsequent sections of this report.

Arising directly from the results reported here, the following programme is suggested:-

(a) That longer term (24 hours) tests at a single combination of creep and fatigue loads be carried out. The combinations of creep and fatigue loads chosen will initially be at $\pm$ 2.5 t.s.i., and 1.5 t.s.i., with static stress greater than 20 t.s.i. at temperatures in excess of 100°C.

(b) All the above specimens will be examined by optical and electron microscopy. Using the Instron machine, small tensile specimens prepared from the remainder of the gauge length can be used to study changes in the mechanical properties brought about by the testing. Of particular interest would be the changes in yield point behaviour.

L_c	F_1	F_2	F_3	F_4	F_5	F_6
tons/ sq.ins.	± 0.1 t.s.i.	± 0.5 t.s.i.	± 1.0 t.s.i.	± 1.5 t.s.i.	± 2.0 t.s.i.	± 2.5 t.s.i.
20.9	0	0	0	0.0020	0.0024	0
22.0	0	0	0	0	0.0003	0.0010
24.0	-0.0015	-0.0012	-0.0006	0	0	0.0012
26.0	0	0.0006	0.0021	0.0020	0.0015	0.0039

Time intervals:- $t_o - t_1$, $t_1 - t_2$ ..... $t_5 - t_6$ all 20 minutes

Units:- ins/ins/hour. Minimum resolution 0.0006 ins/ins/hour. Fatigue frequency 10 C/S

Table 1. Creep rates of RR58 under conditions of constant static loading with incremental fatigue loading at room temperature.

L_c	F_1	F_2	F_3	F_4	F_5	F_6
tons/ sq.ins.	± 0.1 t.s.i.	± 0.5 t.s.i.	± 1.0 t.s.i.	± 1.5 t.s.i.	± 2.0 t.s.i.	± 2.5 t.s.i.
14.0	-	-	0	0	0	0
18.0	0	0	0	0.0010	0.0017	0.0024
20.0	0	0	0.0019	0.0013	0.0032	-
22.3	0	- 0.0021	0.0030	0.0071	0.0150	0.0385

Time intervals:- $t_o - t_1$; ..... $t_5 - t_6$ all 20 minutes

Units:- ins/ins/hour. Fatigue frequency 10 C/S.

Table II Creep Rates of RR58 under conditions of constant static loading with incremental fatigue loading at 130°C.

F_c tons/ sq.ins.	ε_2	ε_3	ε_4	ε_5	ε_6
± 2.5	1.3	1.6	2.9	6.5	
± 1.5	0.8	0.9	1.0	2.4	6.1
± 0.5	0.9	0.6	0.8	1.5	2.7
± 0.1	0.7	0.8	0.6	1.5	2.6

L_1 = 16 t.s.i. L_2 = 18 t.s.i. L_3= 20 t.s.i. L_4= 22 t.s.i. L_5= 24 t.s.i. L_6= 26 t.s.i.

Units:- ins x 10^3./ins.

Time intervals:- $t_o - t_1$, $t_1 - t_2$ ..... $t_5 - t_6$ all 20 minutes

Fatigue frequency 10 C/S

Table III Instantaneous extensions on increasing the static loads on RR58 subject to a combined static and dynamic stress at room temperature.

F_c tons/ sq.ins.	L_1 16 t.s.i.	L_2 18 t.s.i.	L_3 20 t.s.i.	L_4 22 t.s.i.	L_5 24 t.s.i.	L_6 26 t.s.i.
± 2.5	0	- 0.0006	0	0.0013	0	-
± 1.5	0	0	0	0.0006	- 0.0012	0
± 0.5	0	0	0	0	0	0
± 0.1	0	0	0	0	0	0

Units ins/ins/hour: Minimum resolution 0.0006 ins/ins/hour.

Time intervals: $t_o - t_1$, $t_1 - t_2$ .....$t_5 - t_6$ = all 20 minutes.

Fatigue frequency 10 C/S

Table IV Creep Rates of RR58 under conditions of constant fatigue loading and incremental static loading at room temperature.

F_c tons/ sq.ins.	ε_2	ε_3	ε_4	ε_5	ε_6
± 2.5	1.0	1.6	3.6	12.0	30.0
± 1.5	1.0	1.4	3.0	7.0	31.0
± 0.5	1.0	1.0	2.1	3.2	13.0
± 0.1	0.8	1.0	1.3	2.5	7.5

L_1 = 16 t.s.i. L_2 = 18 t.s.i. L_3 = 20 t.s.i. L_4 = 22 t.s.i. L_5 = 24 t.s.i. L_6 = 26 t.s.i.

Units:- ins x 10^3/ins. Time intervals $t_o - t_1$, $t_1 - t$ etc. all 20 minutes.

Fatigue frequency 10 C/S.

Table V Instantaneous Extensions on increasing the static load on RR58 specimens subject to a combined static and dynamic stress at 50°C.

F_c tons/ sq.ins.	L_1 16 t.s.i.	L_2 18 t.s.i.	L_3 20 t.s.i.	L_4 22 t.s.i.	L_5 24 t.s.i.	L_6 26 t.s.i.
± 2.5	0	0.0018	0.	0.0012	0.0060	0.0045
± 1.5	0	0	0	0	0	0.0015
± 0.5	0	0	0	0	0	0.0015
± 0.1	- 0.0015	0	0	0	0	0.0024

Units:- ins/ins/hour. Minimum resolution 0.0006 ins/ins/hour.
20 minutes intervals between increments of static load.

Fatigue frequency 10 C/S

Table VI Creep Rates of RR58 under conditions of constant fatigue loading with incremental static loading at 50°C.

F_c	ε_2	ε_3	ε_4	ε_5	ε_6
tons/ sq.ins.					
± 2.5	1.2	2.4	4.7	15.8	-
± 1.5	0.9	1.2	2.0	5.0	-
± 0.5	0.7	0.75	1.1	2.5	9.0
± 0.1	1.0	1.0	1.5	3.5	8.7

L_1 = 16 t.s.i. L_2 = 18 t.s.i. L_3 = 20 t.s.i. L_4 = 22 t.s.i. L_5 = 24 t.s.i. L_6 = 26 t.s.i.

Units:- ins x 10^3 ins. Time intervals $t_o - t_1$, $t_1 - t_2$ etc. all 20 minutes

Fatigue frequency 10 C/S

Table VII Instantaneous Extensions on increasing the static load on RR58 specimens subject to a combined static and dynamic stress at 75°C.

F_c	L_1	L_2	L_3	L_4	L_5	L_6
tons/ sq.ins.	16 t.s.i.	18 t.s.i.	20 t.s.i.	22 t.s.i.	24 t.s.i.	26 t.s.i.
± 2.5	- 0.0011	- 0.0009	0	0.0009	0.0021	-
± 1.5	0.0009	0	0	0.0009	0.0013	-
± 0.5	- 0.0009	- 0.0009	0	0	0.0009	0.0060
± 0.1	0	0 0.0012	0	0	0	.003

Units: ins/ins/hour. Minimum resolution 0.0006 ins/ins/hour.

20 minutes intervals between increments of static load

Fatigue frequency 10 C/S

Table VIII Creep Rates of RR58 under conditions of constant fatigue loading with incremental static loading at 75°C.

F_c	ε_2	ε_3	ε_4	ε_5	ε_6
tons/ sq.ins.					
± 2.5	0.9	1.8	6.5	13.0	-
± 1.5	2.0	1.8	4.0	6.0	-
± 0.5	0.9	0.9	2.0	4.7	17.0
± 0.1	1.0	1.2	2.0	5.0	17.0

L_1 = 16 t.s.i. L_2 = 18 t.s.i. L_3 = 20 t.s.i. L_3 = 22 t.s.i. L_5 = 24 t.s.i. L_6 = 26 t.s.i.

Units:- ins x 10^3/ins. Time intervals $t_o - t_1$, $t_2 - t_1$ etc. all 20 minutes.

Fatigue frequency 10 C/S.

Table IX Instantaneous Extensions on increasing the static load on RR58 specimens subject to a combined static and dynamic stress at 105°C.

F_c	L_1	L_2	L_3	L_4	L_5	L_6
tons/ sq.ins.	16 t.s.i.	18 t.s.i.	20 t.s.i.	22 t.s.i.	24 t.s.i.	26 t.s.i.
± 2.5	0	0.0009	0	0.0030	0.027	-
± 1.5	0.0011	0	0.0006	0.0024	0.0060	-
± 0.5	0	0	- 0.0012	0	0.0069	0.180
± 0.1	- 0.0015	0	0	- 0.0024	0	0.0180

Units:- ins/ins/hour. Minimum resolution 0.0006 ins/ins/hour.
20 minutes intervals between increments of static load.

Fatigue frequency 10 C/S.

Table X Creep Rates of RR58 under conditions of constant fatigue loading with incremental static loading at 105°C.

F_c	ϵ_2	ϵ_3	ϵ_4	ϵ_5	ϵ_6
tons/ sq.ins.					
± 2.5	1.0	3.0	8.0	12.0	-
± 1.5	1.0	1.5	7.0	-	-
± 0.5	0.9	1.3	3.0		
± 0.1	1.0	1.0	1.1	2.0	16.0

L_1= 16 t.s.i. L_2= 18 t.s.i. L_3= 20 t.s.i. L_4= 22 t.s.i. L_5= 24 t.s.i. L_6= 26 t.s.i.

Units:- ins x 10^3/ins. Time intervals $t_o - t_1$, ...$t_6 - t_5$ etc. all 20 minutes.

Fatigue frequency 10 C/S.

Table XI Instantaneous extensions on increasing the static load on RR58 specimens subject to a combined static and dynamic stress at 120°C.

F_c	L_1	L_2	L_3	L_4	L_5	L_6
tons/ sq.ins.	16 t.s.i.	18 t.s.i.	20 t.s.i.	22 t.s.i.	24 t.s.i.	26 t.s.i.
± 2.5	.0012	.001	0	.012	.045	-
± 1.5	0	- .0006	0.0025	0.0089	-	-
± 0.5	- .0021	0.0015	0.0015	.0030		
± 0.1	0	0	0	0	0.0075	0.180

Units:- ins/ins/hour. Minimum resolution 0.0006 ins/ins/hour.

20 minute intervals between increments of static load.

Fatigue frequency 10 C/S.

Table XII Creep Rates of RR58 under conditions of constant fatigue loading with incremental static loading at 120°C.

F_c tons/ sq.ins.	ε_2	ε_3	ε_4	ε_5
± 2.5	1.2	2.6	4.0	-
± 1.5	1.0	1.1	3.0	-
± 0.5	1.0	0.9	2.0	5.0
± 0.1	1.0	1.5	1.7	4.0

L_1 = 16 t.s.i. L_2 = 18 t.s.i. L_3 = 20 t.s.i. L_4 = 22 t.s.i. L_5 = 24 t.s.i.

Units:- ins x 10^3

Time intervals $t_o - t_1$, $t_1 - t_2$ .... $t_5 - t_6$ all 20 minutes

Fatigue frequency 10 C/S.

Table XIII Instantaneous extensions on increasing the static load on RR58 specimens subject to a combined static and dynamic stress at 130°C.

F_c tons/ sq.ins.	L_1 16 t.s.i.	L_2 18 t.s.i.	L_3 20 t.s.i.	L_4 22 t.s.i.	L_5 24 t.s.i.
± 2.5	0	0	0.0013	0.0111	-
± 1.5	0	0	0.0013	0.0107	0.65
± 0.5	0	0	0.0015	0.0094	0.058
± 0.1	.0015	.0030	0.0021	0.0043	0.018

Units:- ins/ins/hour. Minimum resolution 0.0008 ins/ins/hour.

Time intervals $t_o - t_1$, $t_1 - t_2$.... $t_5 - t_6$ all 20 minutes

Fatigue frequency 10 C/S.

Table XIV Creep Rates of RR58 under conditions of constant fatigue loading with incremental static loading at 130°C.

F_c	ε_2	ε_3	ε_4	ε_5
tons/ sq.ins.				
± 2.5	1.0	2.5	24.0	-
± 1.5	0.8	2.5	6.0	-
± 0.5	1.0	1.1	3.0	-
± 0.1	1.0	1.0	1.7	3.0

L_1 = 16 t.s.i. L_2 = 18 t.s.i. L_3 = 20 t.s.i. L_4 = 22 t.s.i. L_5 = 24 t.s.i.

Units:- ins x 10^3/ins. Time intervals $t_o - t_1$, $t_1 - t_2$ etc. all 20 minutes.

Fatigue frequency. 10 C/S

Table XV Instantaneous extensions on increasing the static load on RR58 specimens subject to a combined static and dynamic stress at 140°C.

F_c	L_1	L_2	L_3	L_4	L_5
tons/ sq.ins.	16 t.s.i.	18 t.s.i.	20 t.s.i.	22 t.s.i.	24 t.s.i.
± 2.5	0	0	0.0030	0.129	-
± 1.5	- 0.0030	- 0.0010	0	0.0175	-
± 0.5	0.0017	0	0.0021	0.015	-
± 0.1	0	0	0	0.0030	0.069

Units: ins/ins/hour. Minimum resolution 0.0006 ins/ins/hour.

20 minutes intervals between increments of static load.

Fatigue frequency 10 C/S

Table XVI Creep Rates of RR58 under conditions of constant fatigue loading with incremental static loading at 140°C.

F_c	ε_2	ε_3	ε_4	ε_5
tons/ sq.ins.				
± 2.5	1.3	2.5	16.0	-
± 1.5	0.9	1.8	4.5	-
± 0.5	1.0	1.0	4.3	-
± 0.1	0.9	1.1	3.5	-

L_1 = 16 t.s.i. L_2 = 18 t.s.i. L_3 = 20 t.s.i. L_4 = 22 t.s.i. L_5 = 24 t.s.i.

Units: ins x 10^3/ins. Time intervals $t_o - t_1$, $t_1 - t_2$ etc. all 20 minutes

Fatigue frequency 10 C/S.

Table XVII Instantaneous extensions on increasing the static load on RR58 specimens subject to a combined static and dynamic stress at 155°C.

F_c	L_1	L_2	L_3	L_4	L_5
tons/ sq.ins.	16 t.s.i.	18 t.s.i.	20 t.s.i.	22 t.s.i.	24 t.s.i.
± 2.5	0.0009	0	0.0042	0.468	-
± 1.5	0.0012	0.0027	0.0024	0.078	-
± 0.5	- 0.0012	0	0	0.027	-
± 0.1	0.0015	0.0013	0.0015	0.011	-

Units: ins/ins/hour. Minimum resolution 0.0006 ins/ins/hour.

20 minute intervals between increments of static load.

Fatigue frequency 10 C/S.

Table XVIII Creep Rates of RR58 under conditions of constant fatigue loading with incremental s tatic loading at 155°C.

Change in max.stress	18.5→20.5	20.5→22.5	22.5→24.5	24.5→26.5
RT (a)	1.3	1.6	2.9	6.5
RT (b)	0.6	0.8	1.5	2.7
50° (a)	1.0	1.6	3.6	12.0
50° (b)	1.0	2.1	3.2	13.0
75 (a)	1.2	2.4	4.7	15.8
75 (b)	0.75	1.1	2.5	9.0
105 (a)	0.9	1.8	6.5	13.0
105 (b)	0.9	2.0	4.7	17.0
120 (a)	1.0	3.0	8.0	12.0
120 (b)	1.3	3.0	-	-
130 (a)	1.2	2.6	4.0	-
130 (b)	0.9	2.0	5.0	-
140 (a)	1.0	2.5	24.0	-
140 (b)	1.1	3.0	-	-
155 (a)	1.3	2.5	16.0	
155 (b)	1.0	4.3	-	-

a. Fatigue ± 2.5 tons/sq.ins.

b. Fatigue ± 0.5 tons/sq.ins.

TABLE XIX Instantaneous extensions in RR58 on changes in the maximum total stress for two levels of fatigue stress.

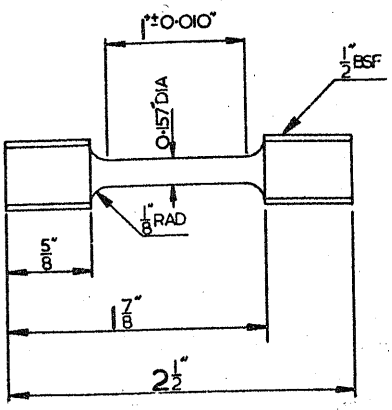

Figure 6

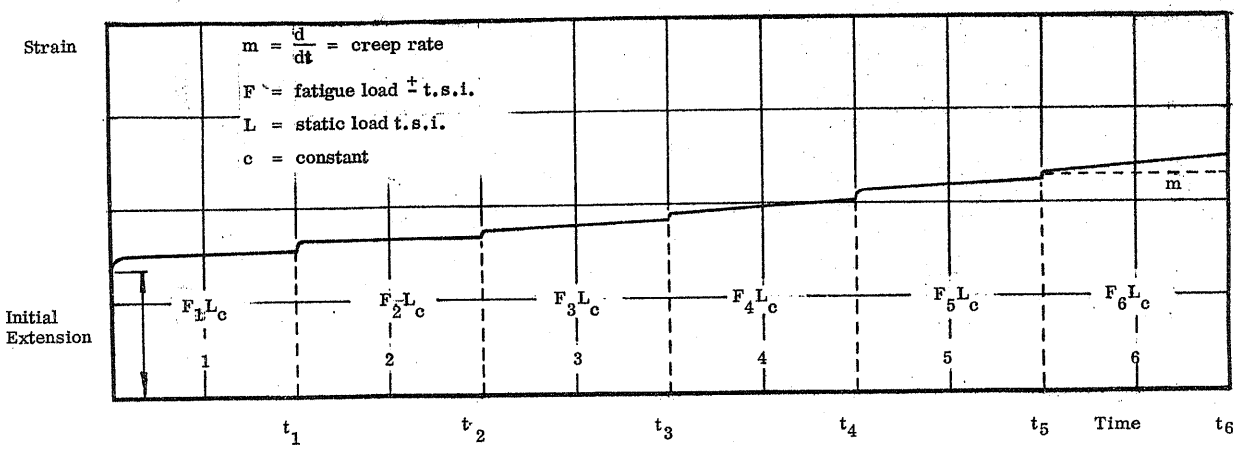

Figure 7

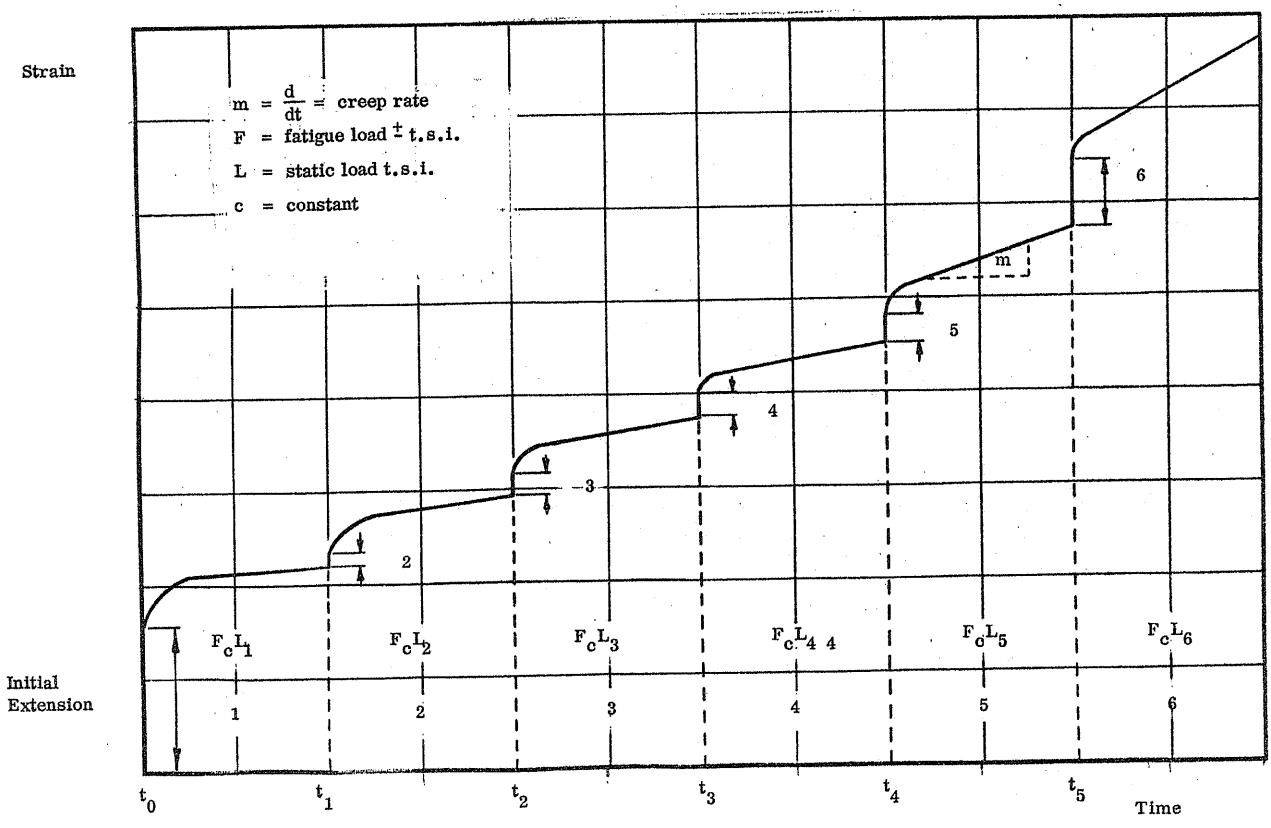

Figure 8

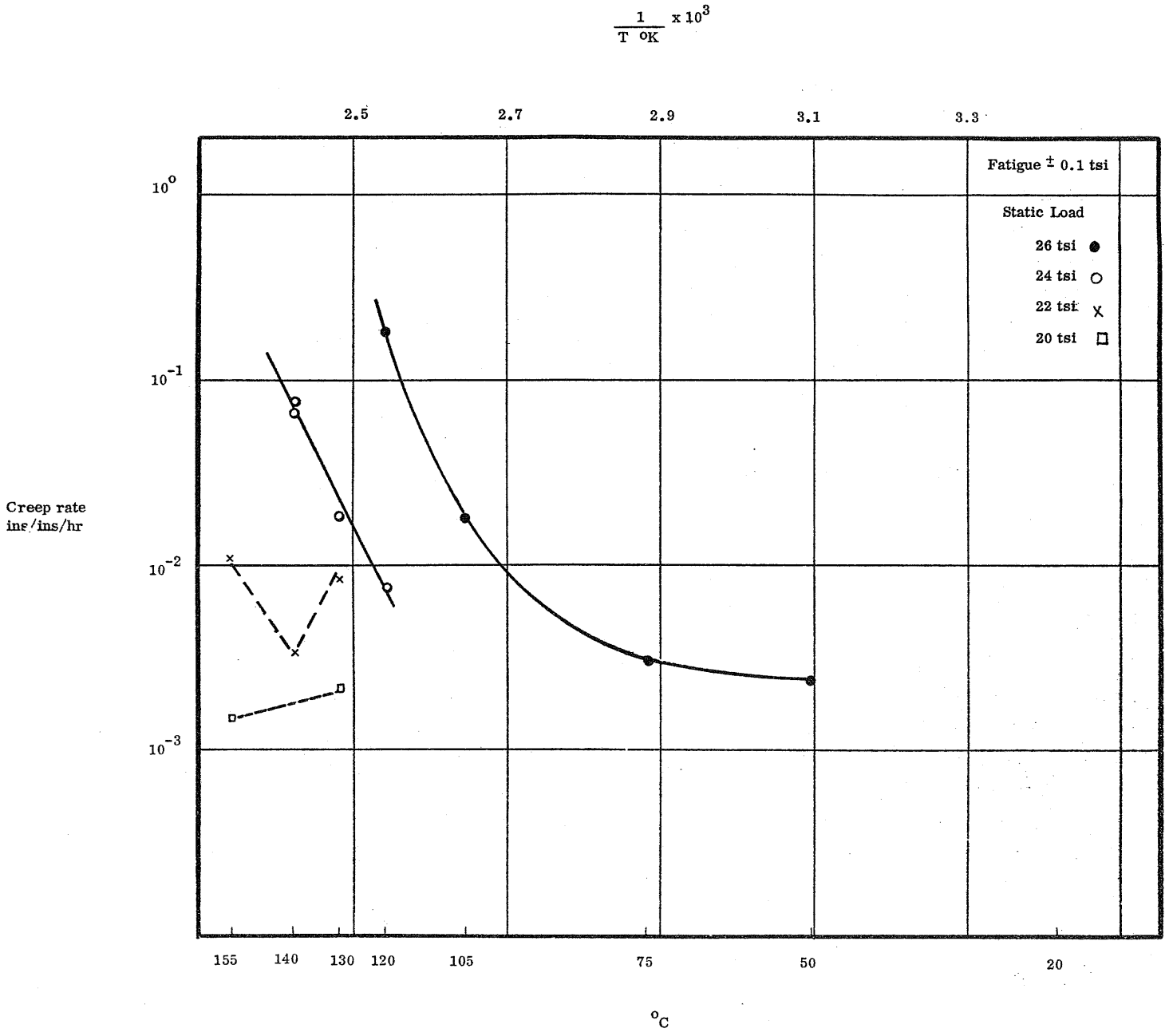
$\frac{1}{T\ ^oK} \times 10^3$
2.5
2.7
2.9
3.1
3.3
Fatigue ± 0.1 tsi
Static Load
26 tsi
24 tsi
22 tsi
20 tsi
10^0
10^{-1}
10^{-2}
10^{-3}
Creep rate
ins/ins/hr
155
140
130
120
105
75
50
20
^oC

Figure 9

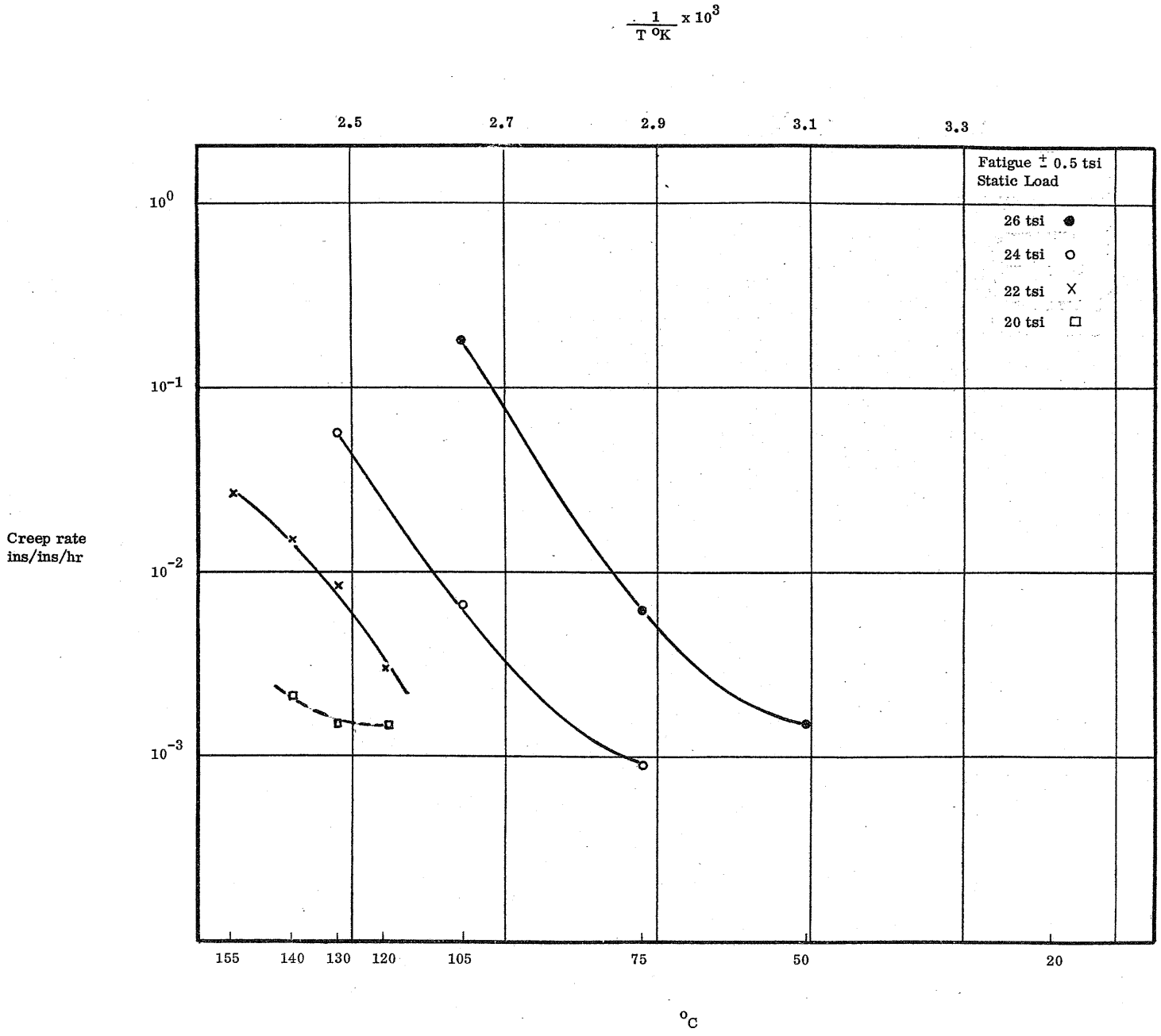
$\frac{1}{T\ ^oK} \times 10^3$
2.5
2.7
2.9
3.1
3.3
Fatigue ± 0.5 tsi
Static Load
26 tsi
24 tsi
22 tsi
20 tsi
10^0
10^{-1}
10^{-2}
10^{-3}
Creep rate
ins/ins/hr
155
140
130
120
105
75
50
20
^oC

Figure 10

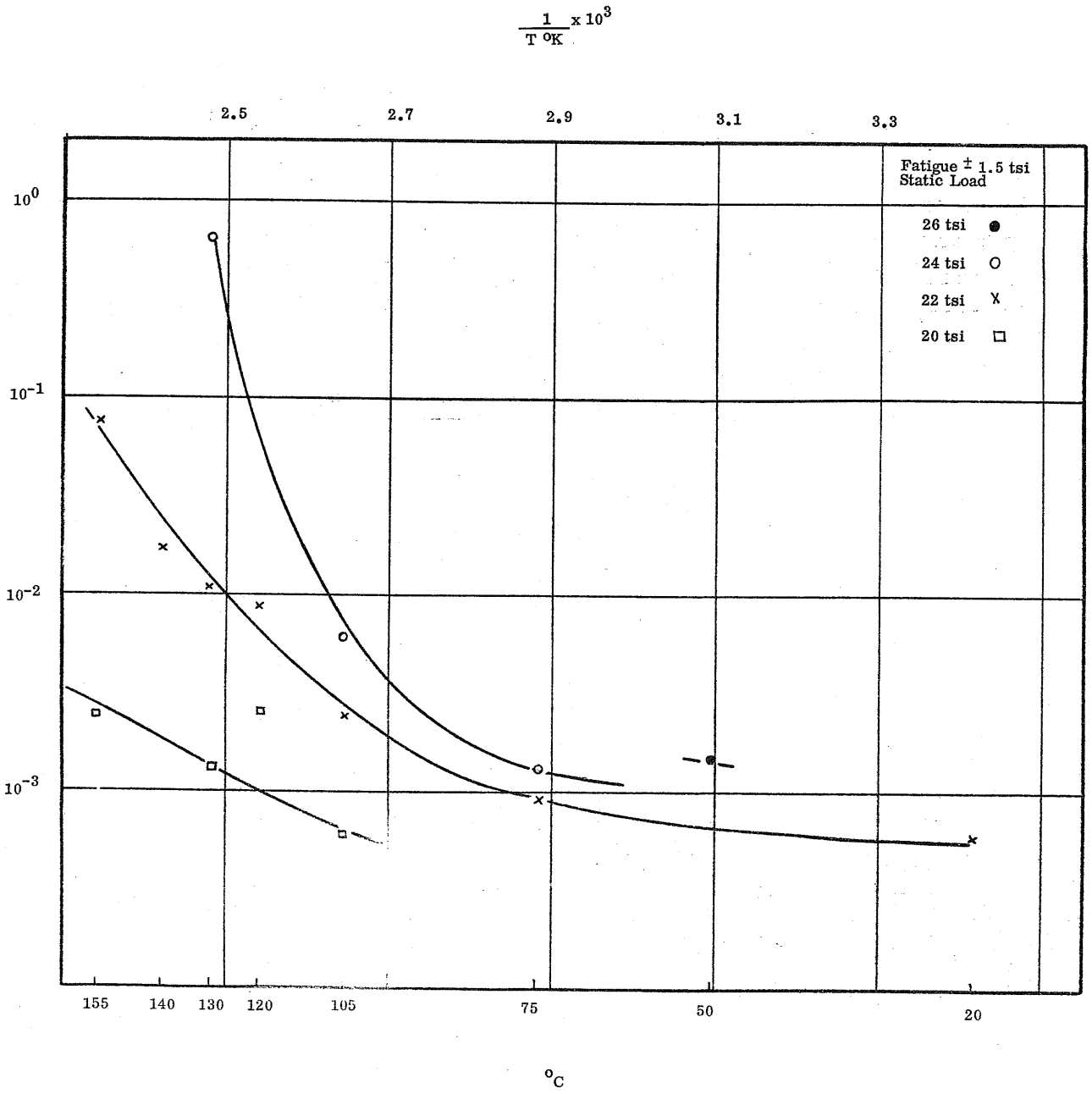
$\frac{1}{T\ ^oK} \times 10^3$
2.5
2.7
2.9
3.1
3.3
Fatigue ± 1.5 tsi
Static Load
26 tsi
24 tsi
22 tsi
20 tsi
10^0
10^{-1}
10^{-2}
10^{-3}
Creep rate
ins/ins/hr
155
140
130
120
105
75
50
20
^oC

Figure 11

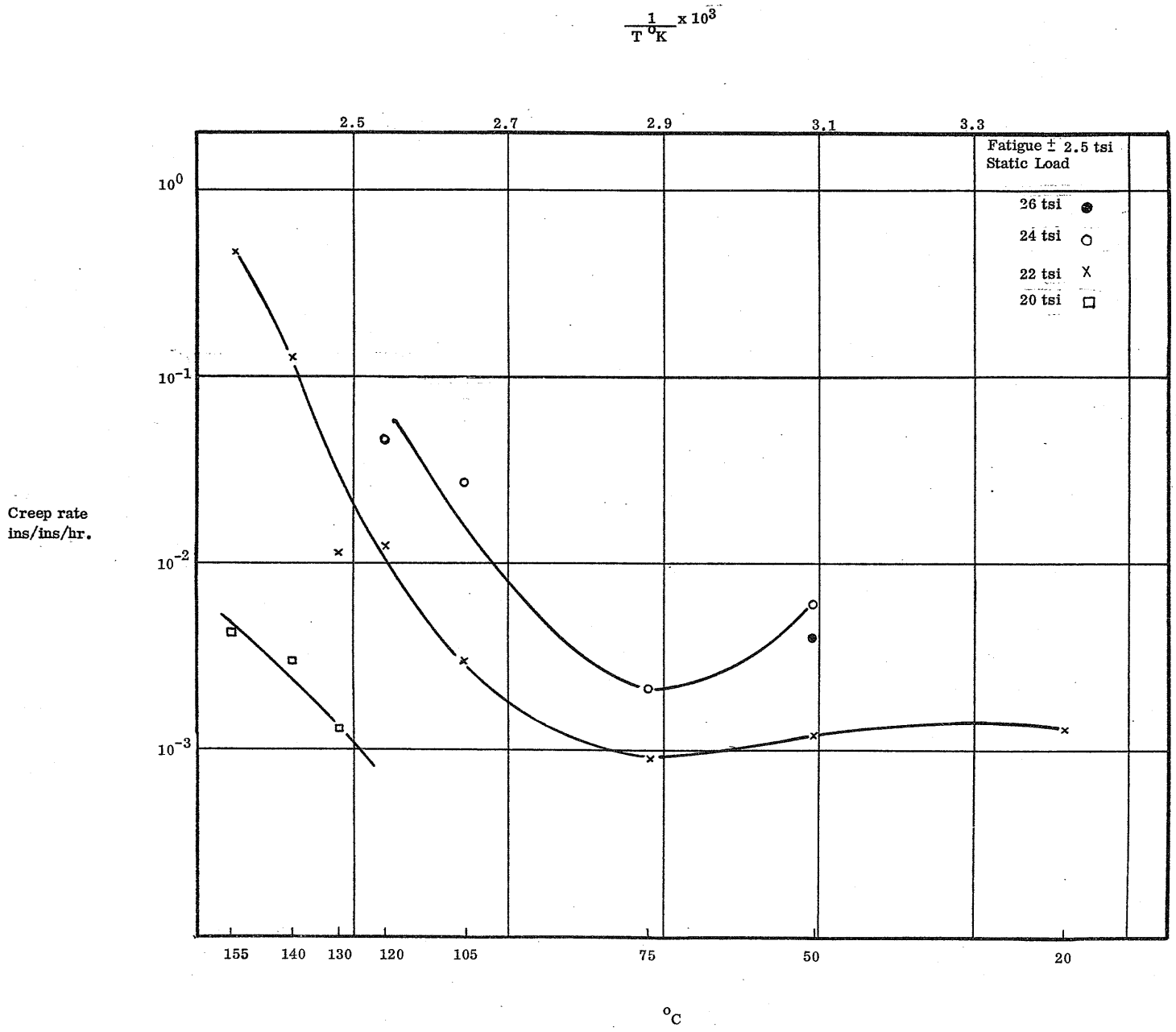
$\frac{1}{T\ ^{o}K} \times 10^{3}$
2.5
2.7
2.9
3.1
3.3
Fatigue ± 2.5 tsi
Static Load
26 tsi
24 tsi
22 tsi
20 tsi
10^{0}
10^{-1}
10^{-2}
10^{-3}
Creep rate
ins/ins/hr.
155
140
130
120
105
75
50
20
^{o}C

Figure 12

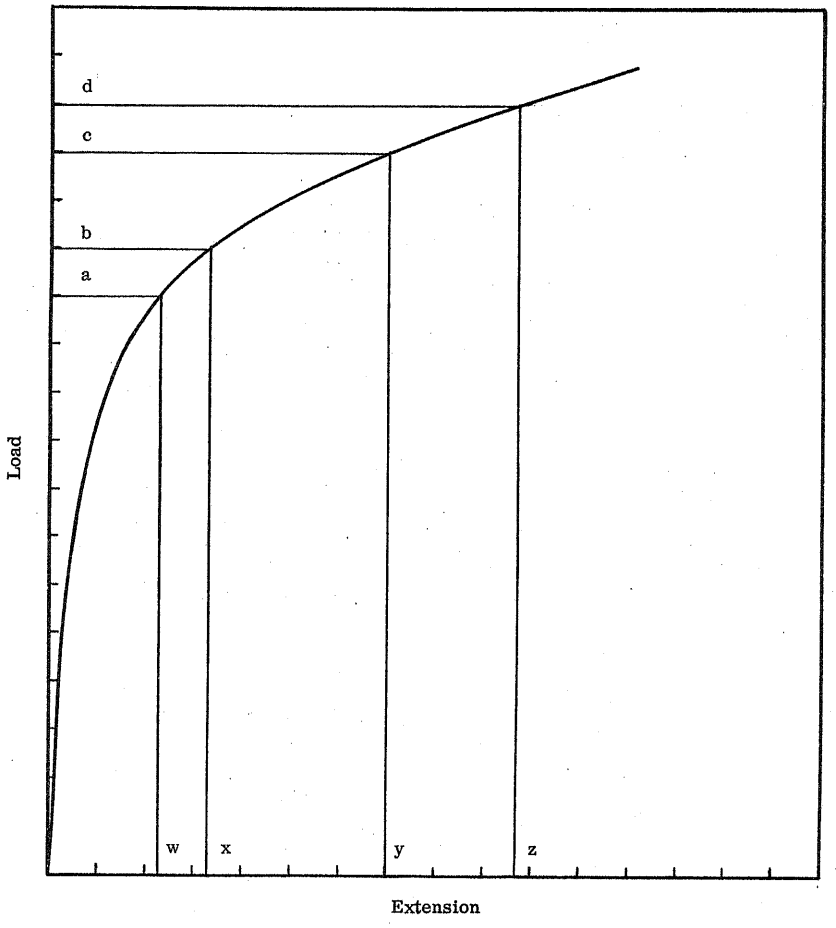

Figure 13

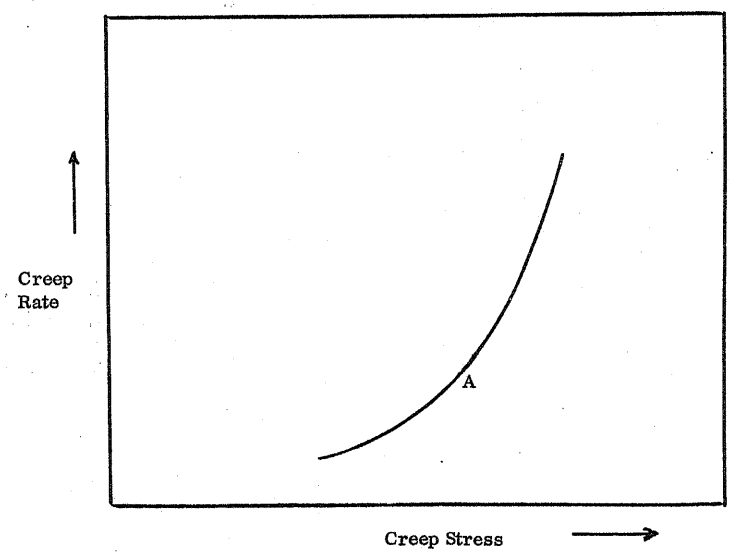

Figure 14

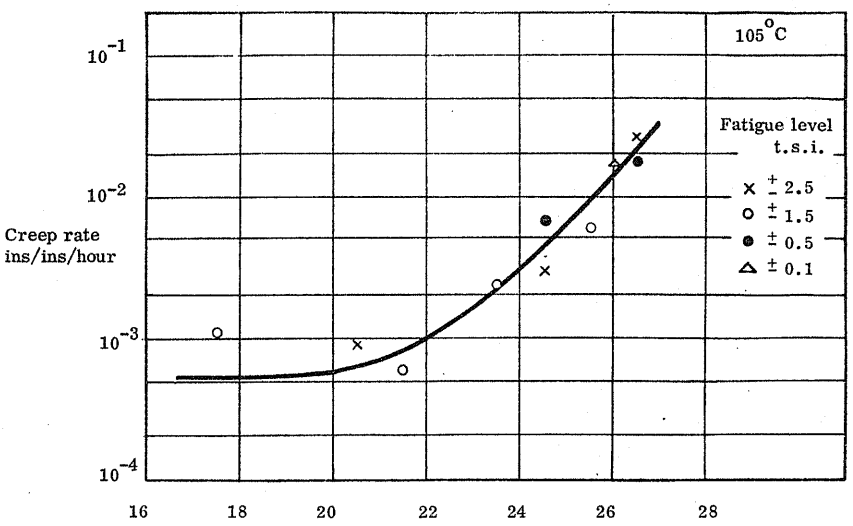

Figure 15

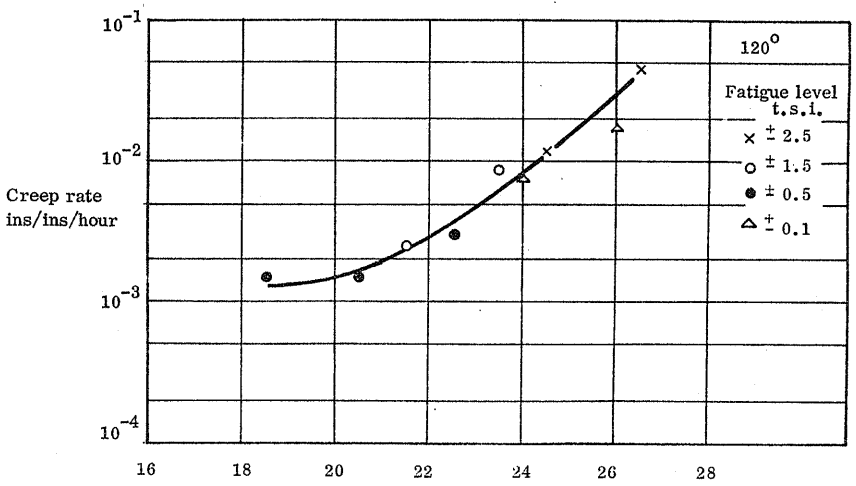

Figure 16

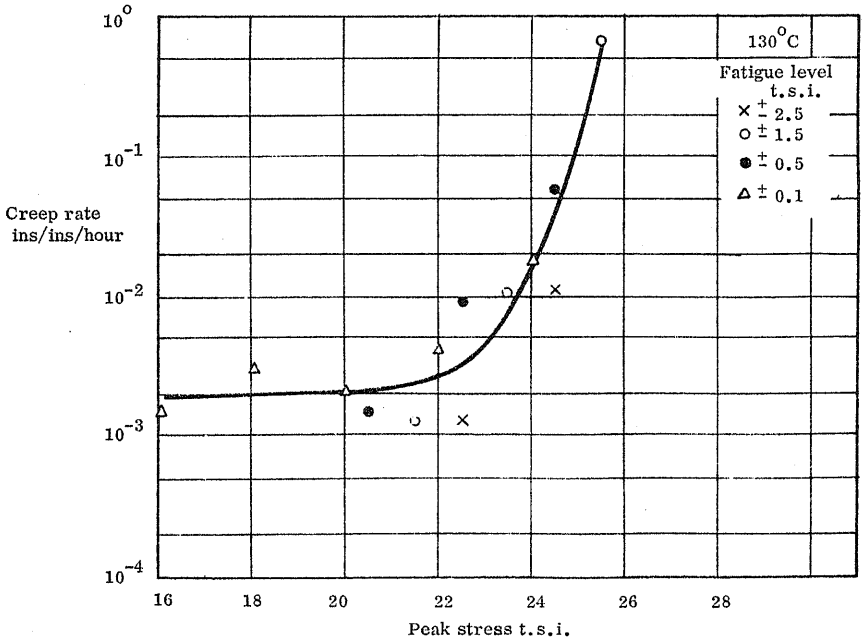

Figure 17

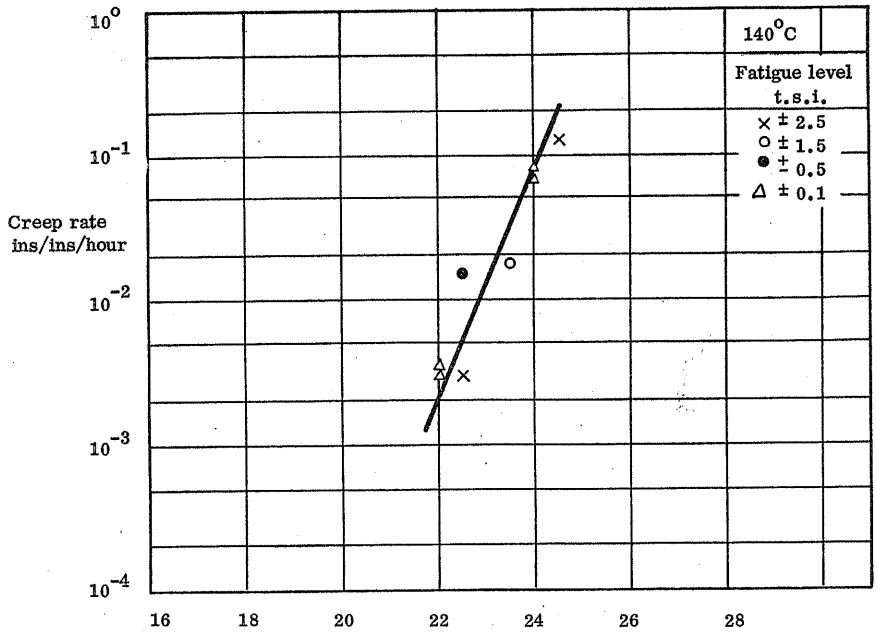

Figure 18

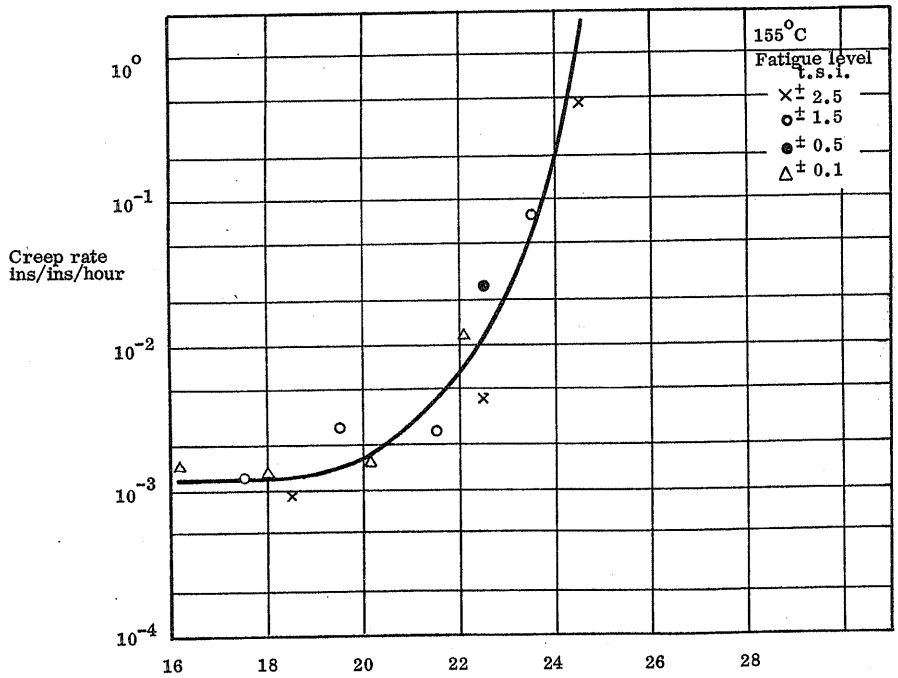

Figure 19

Part III

Structural aspects of combined creep and fatigue testing including the effects of a low number of cycles

by

R.G.C. Hill, B.A., B.Sc.

COLLEGE OF AERONAUTICS LIBRARY

1. Introduction

The experiments described in the following sections have been carried out with the object of investigating the substructures produced by the various testing conditions imposed upon the specimens.

Three techniques have been applied:-

(i) tensile measurements
(ii) optical metallography of electropolished surfaces
(iii) electron metallography of the bulk specimens

The technique of subsequently testing the push-pull fatigue specimens in tension has been used by Broom and Ham (1957) on polycrystalline copper, and later (1959) on copper single crystals of several orientations; in the latter work the results clearly distinguished between the properties of the fatigue slip striations and the relatively hard matrix.

The principal interest in studying the surfaces of the specimens lies in the slip markings, and in the fatigue tested specimens, the fatigue slip striations (or "persistent slip lines"). Experimental evidence gained from this technique and the more quantitative results of tensile testing should provide a good correlation with the electron metallography.

2. Experimental

(a) Heat treatment

The specimens used for the creep and fatigue testing were heat treated in the form of $\frac{1}{2}$ inch extruded rod before machining. The treatment consisted of a 4 hours solution treatment at 530°C, followed by 10 seconds air cool and water quench; the ageing treatment was 20 hours at 190°C.

The other specimens were machined in the as-received condition and heat treated afterwards; all except 38 - 47 (Instron) were heat treated under the same conditions as the creep and fatigue specimens. Specimens 38 - 47 were quenched immediately from the solution treatment temperature, otherwise the treatment was identical.

All specimens which were tested in the fully heat treated condition will be termed "heat treated" (or "as received", which material was in the fully aged condition), to distinguish them from the solution treated specimens which were treated at 530°C for 4 hours and quenched. Specimens 13 - 32, even though

nominally given the same heat treatment as the others, were of lower strength.

(b) Fatigue testing

(i) Creep plus fatigue

Combined creep and fatigue testing was carried out in tension in the hydraulic creep and fatigue machine. The specimens, of 1" gauge length, were tested as machined, and at temperatures above room temperature a thermocouple was welded to the middle of the gauge length to facilitate accurate temperature measurement. However, this method of attachment probably had little effect on the test behaviour, since these specimens which were fractured never fractured at the point of attachment of the thermocouple. The frequency used in all tests was 10 c.p.s.

(ii) Fatigue

A 2 ton Amsler Vibrophore was used for the push-pull fatigue tests and for the room temperature tension fatigue tests. The specimens used had a cylindrical gauge length with radiused ends and the testing frequency was 160 c.p.s.

All specimens were electropolished in Lenoir's solution. (Lenoir 1953).

(c) Tensile testing

(i) Hounsfield tests

An autographic recording Hounsfield tensometer was used for most of the tensile tests on the creep and fatigue tested specimens, at a strain rate of 0.060 min.$^{-1}$. The specimens used for the simple tensile experiments and for the low cycle tests were also of 1 inch gauge length.

Low cycle tension fatigue treatments were carried out by hand in the tensometer by adjusting the load between two predetermined limits for a given number of cycles, in which case the stress was always relaxed to zero before subsequent tensile testing, also at a strain rate of 0.06 min.$^{-1}$.

All specimens used (apart from those which had been creep and fatigue tested in the hydraulic machine) were electropolished in Lenoir's solution.

(ii) Instron tests

The later tests were carried out using an Instron Universal Tensile Testing machine, which allows stress cycling between two fixed limits to be carried out automatically. The strain rate chosen was 0.050 min.$^{-1}$, both for the straight tensile tests and for the stress cycling.

The specimen surfaces were prepared in the same way as in (i) above.

(d) Optical metallography

The electropolished surfaces of specimens were examined after testing with a Reichert Universal camera microscope and photographed at a magnification of 400 x.

(e) Electron metallography

Specimens were examined by the technique of thin foil electron microscopy in a Siemens Elmiskop 1 electron microscope operating at 100 kv.

The foils were prepared by electropolishing small discs of the material in a 10% solution of perchloric acid in ethanol. The discs were produced by slicing up the gauge lengths of the specimens in a Buehler cut-off machine and then electromachining a small depression on each side with a jet of 30% nitric acid. This latter operation ensured that the thinned part would be located at the approximate centre of the disc.

3. Results

3.1 Tensile

(a) Stress-strain curve at 20°C

Figures 1 and 2 show stress-strain curves of the "heat treated" material, the points marked on the curve in Figure 1 correspond to the positions at which the surface markings were examined microscopically. The curve shows a steep initial rate of work-hardening, there being no sharply defined

yield point. In the following sections the flow stress will be taken as the departure from the extended elastic line ("departure from linearity", or "D.F.L.") in order to differentiate from what will be called a "yield point" - a sharply defined knee in the curve.

The rate of work-hardening can be seen to decrease continuously until the U.T.S. is reached, when there is an appreciable horizontal portion before necking sets in and the curve falls to fracture.

Figures 10 and 11 show tensile curves of the solution treated specimens. Again there is no definite yield point, and the general shape of the curve is comparable to that of the "heat treated" specimens, although the strength values are, of course, lower. The curves indicate that "jerky flow" has taken place, and the fracture was shear rather than the "cup-and-cone" of the heat treated specimens.

(All these tensile curves are uncorrected for the deflection of the load-beam).

(b) Examination of surface markings

Figures 3 - 9 show micrographs of the electropolished surfaces of tensile specimens and Figure 3 an unstrained specimen.

Slip markings grow more pronounced with increasing strain and at 3% strain, two intersecting slip systems are operative.

It appears that some localized grain boundary cracking may occur in boundaries orientated approximately at right angles to the tensile axis. At 3% strain these "cracks" seem to have started at inclusions, and at the U.T.S. quite long cracks can be seen. It is not certain from these micrographs whether these are actual cracks or merely heavy distortion of the grain boundary regions.

(c) Low cycle fatigue, experiments at 20°C

(i) Hounsfield tests

Figures 12 - 20 show typical tensile curves of low cycle results for 1 and 100 cycles.

All the curves in which the maximum stress has exceeded the original D.F.L. of the material show two distinct features: (i) the curve departs from the extended elastic line at a value which is at approximately that of

the maximum stress reached in the cycle, and (ii) thereafter, depending on the maximum stress, the curve rises to the U.T.S., or, with high maximum stresses, is flat topped and falls when necking of the specimen occurs, to fracture. Sometimes irregularities or "jerks" are shown in the work-hardening curves.

The main points of interest of these experiments, seem to be the relative values of the D.F.L. and Y.P. to the maximum stress in the fatigue treatment, depending on such factors as the value of the maximum stress, and the duration of the period between the fatigue treatment and tensile testing; and the appearance or non-appearance of "jerks" in the work-hardening curve.

For both 1 cycle and 100 cycle treatments, on immediate tensile testing the D.F.L. was within the limits of experimental error coincident with the maximum stress of the pre-treatment (referred to hereafter as simply maximum stress).

On resting at 20°C for 4 - 5 hours, the D.F.L. fell to a value below the maximum stress. On resting for 5 minutes, at 100°C the D.F.L. was also lowered significantly below the maximum stress.

The yield point (the knee in the curve) on resting at 20°C for 4 - 5 hours was approximately at the same value as the maximum stress. On immediate testing, the yield point was appreciably above the maximum stress. On 5 minutes resting at 100°C the yield points appeared to be at the same values as for immediate re-testing.

In the tests of Figure 18 and 19, the U.T.S. appeared to be lower than the maximum stress, and although this might have been an experimental mistake, more probably necking occurred during the cycling since, in the final tensile test, the curve falls immediately once the knee has been reached.

Several specimens showed a yield plateau and a few even a slight yield drop, e.g. Figure 14. The specimens whose tests are shown in Figures 15 and 17 showed a very long yield plateau. Figures 17 and 20 show slight jerking.

(ii) Instron tests

The greater sophistication of this machine enabled similar experiments to those performed on the Hounsfield tensometer to be executed more accurately and with more certainty.

Figures 21 - 29 show cycling curves and the tensile curves obtained for a range of three maximum stresses within the plastic range.

The results can be summarized as follows:

A. Rested 20 hours at 20°C after cycling

1 cycle

D.F.L. Below the maximum stress, the amount of the lowering increasing with the maximum stress; the pre-yield strain certainly increased quite markedly with the maximum stress.

Y.P. Raised slightly. In fact the value seemed to be the same as that which occurred in the 100 cycle tests, even though the maximum stress for 1 cycle was lower than for the 100 cycle tests. This was due to plastic creep occurring allowing the machine to cut off at, or very little above, the set maximum stress, instead of overshooting. (A cam operates a microswitch at the stress limits, and due to mechanical delay on reversal, overshooting is unavoidable.)

U.T.S. Unaltered.

100 cycle

D.F.L. The same as for the 1 cycle tests.

Y.P. Raised slightly above the maximum stress.

U.T.S. Unaltered.

1,000 cycles

One test was carried out, the rest period being 24 hours at 20°C.

D.F.L. This was below the maximum stress, and the pre-yield was much smaller than for the 1 and 100 cycle tests.

Y.P. Lowered appreciably below the maximum stress.

U.T.S. Unaltered.

B. Immediate re-tests

1 cycle

D.F.L. Markedly higher than in rested specimens, but still below the maximum stress, and the pre-yield strain was very small.

Y.P. Raised, but slightly lower than in the 100 cycle tests.

U.T.S. Unaltered.

100 cycle

D.F.L. The same as for the 1 cycle tests.

Y.P. Raised, probably little higher than in rested specimens, but slightly below that of the rested 1,000 cycle test at the same maximum stress.

U.T.S. Unaltered.

Marked jerking appeared at the highest maximum stress values and seemed to be similar in the 1 and 100 cycle tests. The jerk period followed a yield plateau and occurred in steps joined by level portions.

Immediate re-testing seemed to give smaller jerks than the 20 hours rested specimens and in the 1,000 cycle tests jerking was markedly less pronounced. The yield point was followed by a very small yield plateau.

(d) Tensile tests of creep and fatigue tested specimens

(i) Hounsfield tests

Since the rest periods from fatigue treatment to tensile testing were variable, and the calibration of the fatigue machine and the tensile machines could obviously not be identical, little or nothing can be drawn from the relative values of the stresses.

Some specimens showed slight yield plateaus (i.e. Figures 33, 34 and 35). All curves which have a knee, except Figure 32, show a pronounced pre-yield strain.

Some curves show jerking, i.e. Figures 30, 31, 34 and 35 and these jerks appear not to be merely the limits of yield plateaus, as seems to be the case in the low cycle experiments, but kinks superimposed upon the work-hardening curve.

(ii) Instron tests

The pre-yield extensions were also considerable in the tests shown in Figures 36 - 40 (all rested for several weeks at 20°C). Thus the D.F.L. was markedly lower than the Y.P. Only one or two tests showed any real jerking i.e. Figure 37 (which also showed a "reverse jerk"), Figures 39 and 40.

(e) Tensile tests of push-pull fatigue and tension fatigue tests at 20°C

The maximum stress reached in each of these tests was designed never to exceed significantly the D.F.L. of the material. The tensile results (Figure 41) all show the same kind of curve obtained in virgin material, which indicates that, at least for the number of cycles used, fatigue stressing below the D.F.L. produces no very appreciable differences in tensile behaviour.

3.2 Metallographic

(a) Optical examination of the surfaces of push-pull fatigue specimens

Figures 42 - 50 show micrographs of the electropolished surfaces of fatigue specimens stressed under the various conditions stated. It is apparent that at stresses little below the yield point cracking was partly intergranular and partly transgranular, slip striations can be seen on many grains, but no "persistent slip lines".

The structure of the specimen stressed at $\pm$ 10 t.s.i. appeared to be undistorted away from the fracture edge, no striations being visible, and no cracks. The fracture was wholly transgranular.

The specimen, stressed at $\pm$ 5 t.s.i., had a structure which showed "persistent slip lines" (Figures 48 - 50), but it seems that the cracks probably did not start from these, although in Figure 50 a crack has either run along one after starting at an inclusion or has started in the persistent slip line itself and the presence of the inclusions has helped in its propagation.

(b) Electron metallography

As a result of the technique of preparation of the thin foils, their surfaces were contaminated with etch products, and these appear as small spots on the micrographs. These spots were thought to lie on the surface because, firstly, their contrast was the same whether they lay within an extinction contour or not, and, secondly, if a micrograph was taken of an area, and this compared with another micrograph taken after the specimen had been tilted slightly, it appeared that one "set" of spots had moved by the same amount relative to another set, indicating that each set lay in the same plane.

(i) As received RR58

Figure 51 shows a grain boundary with a bend extinction contour crossing it (the grain size was approximately 100 microns); the contamination can be seen as spots scattered evenly over the surface and it seems that they are probably formed as a result of the preferential etching away of precipitate particles which intersect the surface of the foil. The precipitate particles are rod-like and, from selected area diffraction, evidence lies in $\langle 100 \rangle$ directions; they are about 0.5 to 0.75 microns in length.

It seems that the particles are surrounded by strain fields (see, e.g., Figure 52), where several particles within the extinction contour show an intense dark line on either side of them, and one or two of them show shaded contrast indicating that the strains extend for an appreciable distance from the particles.

Individual dislocations are not evident in these micrographs. On examination of the foils their density seemed low, although occasional movements were observed.

(ii) Heat treated RR58 (4 hours solution treatment at 530°C, (10 seconds air cool, 20 hours aged (at 190°C.

In this condition, the grain size of the material was approximately 200 microns, although sub grains were also present of size about 5 microns (Figure 53). The orientation across the sub-grain boundaries was small since selected area diffraction patterns taken on either side of the sub-boundaries could be indexed similarly.

The general precipitation was very much finer than in the as received material and the particles were only just resolvable, (Figure 54). In this figure much coarser particles can also be seen and a general feature seems to be these "stacks" of coarse particles (Figures 53 - 56). In Figure 53 the stacks are located both within the sub-grains and at their boundaries. The size of these coarse particles is about 0.5 micron. Often the "stacks" appears as zig-zags, (Figure 53) remiscent of a helix seen sideways on. On examination it is seen that the "stacks" are really composed of parallel lines (Figure 57) arranged so as to give a zig-zag appearance. Similar observations have been made in high purity Al-Cu-Mg alloys by Vaughan, who attributed the effect to preferential precipitation on an helical dislocation.

Selected area diffraction indicated that the parallel lines (precipitate particles) lie in $\langle 100 \rangle$ directions (Figures 58 and 59).

In general, dislocations seemed to be concentrated at the sub-boundaries (Figure 60), and the grains themselves appeared to contain a relatively low density of dislocations.

(iii) RR58, heat treated, and subjected to 17.5 t.s.i. static stress with a superimposed fatigue stress of $\pm$ 2.5 t.s.i. at 130°C.

Sub-grains are again present in this material and they are of the same size as in the material which has not been subjected to creep.

The zig-zags are again present, and also what appear to be helical dislocations themselves, rather than precipitation effects on dislocations (Figures 61 and 62). In Figure 61 several other irregular dislocations can be seen, but the irregularities might be caused by "dotted" and "wavy" contrast effects; on the other hand, a $\langle 100 \rangle$ direction lies very close to the zone axis and thus the dotted effect might be caused by precipitate particles lying in this direction and consequently seen nearly end-on.

The general dislocation density seems much higher than in the heat treated material (Figures 63 and 64). A large loop is visible in Figure 65 and possibly a few small loops at the bottom left hand corner of the micrograph; a $\{111\}$ plane lies very nearly in the plane of the foil, thus it is highly probable that they lie in this plane.

Figures 65 and 61 show a sub-boundary (these were observed in the uncrept material as well); coarse precipitation can be seen in the boundary, and it is clear that the precipitates lie in the $\langle 100 \rangle$ directions.

(iv) RR58, heat treated, and subjected to 14.75 t.s.i. static stress with superimposed fatigue stress of $\pm$ 0.3 t.s.i. (no creep after 5 hours) at 130°C.

The structure appeared the same as the heat treated material, and the dislocation density was equivalent. Figure 66 shows a main grain boundary with a sub-boundary branching off. Figures 67 and 68 show a sub-boundary with the precipitate particles lying in the boundary clearly revealed. At the point marked in Figure 68, it appears that the precipitate particles have nucleated on a dislocation and are here seen end-on (a $\langle 100 \rangle$ lies very near to the zone axis).

4. Discussion

(a) Tensile properties at 20°C

The form of the curve of the heat treated material is typical of an age hardened alloy in showing a high yield strength to ultimate tensile strength ratio; hence the limitation on the amount of plasticity available.

The indication given by the optical micrographs that some localized grain boundary cracking occurs is surprising, and especially since they seem to occur very early in the test. The conclusion that they are cracks is confirmed by the fact that they appear only in those grain boundaries orientated at right angles to the gauge length of the specimens, whereas boun daries at right angles to the tensile axis appear unchanged.

Inclusions are favourable initiation points for cracks, but unless there was an inherent grain boundary weakness the cracks would not be expected to propagate further. A grain boundary weakness could certainly be caused by either a precipitate denuded zone or a coarsening of the precipitate particles at the grain boundaries. The cracking is probably a surface effect since an inclusion lying at the surface is an obvious point of weakness; the slight etching away of the grain boundaries during the electropolishing might also have assisted cracking. The fact that the final failure was of normal "cup and cone" type also indicates that the cracks were confined to the surface.

The phenomenon of "jerky flow" (or the Portevin-Le Chatelier effect) which was shown by the solution treated specimens is best known in aluminium alloys, especially those containing magnesium. It is usually attributed to the breakaway of dislocations from atmospheres of solute atoms which diffuse to them during the course of the test. In order to explain the high rate of diffusion necessary it is also suggested that vacancies produced during the straining assist the diffusion of the solute atoms.

The slightly higher strength values, and the smaller elongation of the specimen tested at the lower strain rate, as well as the shear fractures of the specimens, suggest that ageing occurred during the course of the tests.

(b) Low cycle fatigue experiments at 20°C

The experiments show that there was very little, if any, difference between the tensile curves obtained from specimens which had been subjected to 1 and 100 cycles. This is surprising since the amount of strain introduced into the 100 cycle specimens was greater than in the 1 cycle, since the peaks in the load elongation curves (Figures 21 - 29) do not attain a constant value until the

fourth or fifth cycle. Thus, as explained in section 3 (c)(ii), plastic strain must still occur until a constant load value of the peaks has been reached.

The relative values of the D.F.L. and Y.P. to the maximum stress in the fatigue cycle after the various rest periods indicate that time-dependent relaxation has occurred. Relaxation effects are, of course, important in creep and fatigue tests since they determine the amount of strain in the cycle. The reason why the relaxation effect is much larger after the low cycle tests is that the stress was relaxed below the minimum stress in the cycle (to zero) before subsequent tensile testing.

Nevertheless the experiments have demonstrated a possible means of approach to the sequence of events in each cycle of normal creep and fatigue experiments.

The jerking that was observed in some of these tests differed from normal yield behaviour in that it proceeded in a series of steps joined by straight line portions. An obvious comparison can be made with the "jerky flow" but, as can be seen in Figures 10 and 11, the stress drops after each jerk to the extended work-hardening curve.

(c) Tensile properties of creep and fatigue tested specimens

The jerking of some of these specimens was much more like that observed in the solution treated specimens, although only a few specimens showed this phenomenon. Probably the rest periods after the fatigue testing were important since these varied from specimen to specimen.

The phenomenon might be explained by the same theory described in 4(a), although the free solute concentration in the age hardened alloy would be very much smaller than in the solution treated condition. However the number of vacancies produced in a creep and fatigue test (in the plastic range) might be sufficiently large to allow the diffusion of enough solute atoms to dislocations to lock them. Some obvious further experiments which suggest themselves are the examination of the effects of rest periods after fatigue testing before tensile testing, and the behaviour of solution treated, and partially aged material.

(d) Optical examination of push-pull fatigue specimens

This examination showed that cracks produced by fatigue stressing were partly transgranular and partly intergranular. Considering the tensile results, intergranular cracking is not surprising, although cracks were probably not initiated directly in grain boundaries.

Cracks in the specimen stressed at $\pm$ 5 t.s.i. were probably initiated in persistent slip lines since in Figure 48 a large grain can be seen in which several such lines have cracked, although inclusions would also be expected to be favourable crack nucleation points.

(e) Electron metallography

The marked difference in structure of the as received material and the "heat treated" material is presumably a result of the short air cool following solution treatment. This presumably allows preferential nucleation on helical dislocations and hence leads to the "stacks" of coarse particles. The very fine general precipitation is probably a result of the partial denudation of the rest of the matrix.

The specimen which had crept during the creep and fatigue treatment showed a relatively high denisty of dislocations, although only a few loops were seen, and there appears to be a helical dislocation in Figure 61.

References

1. T. Broom and R.K. Ham, Proc. Roy. Soc. A. 242, 1957, 166.

2. T. Broom and R.K. Ham, Proc. Roy. Soc. A. 251, 1959, 186.

3. G. Lenoir, Rech. Aeronautique, 36, 1953, 35.

4. D. Vaughan, unpublished.

5. A.H. Cottrell, Phil. Mag. 44, 1953, 829.

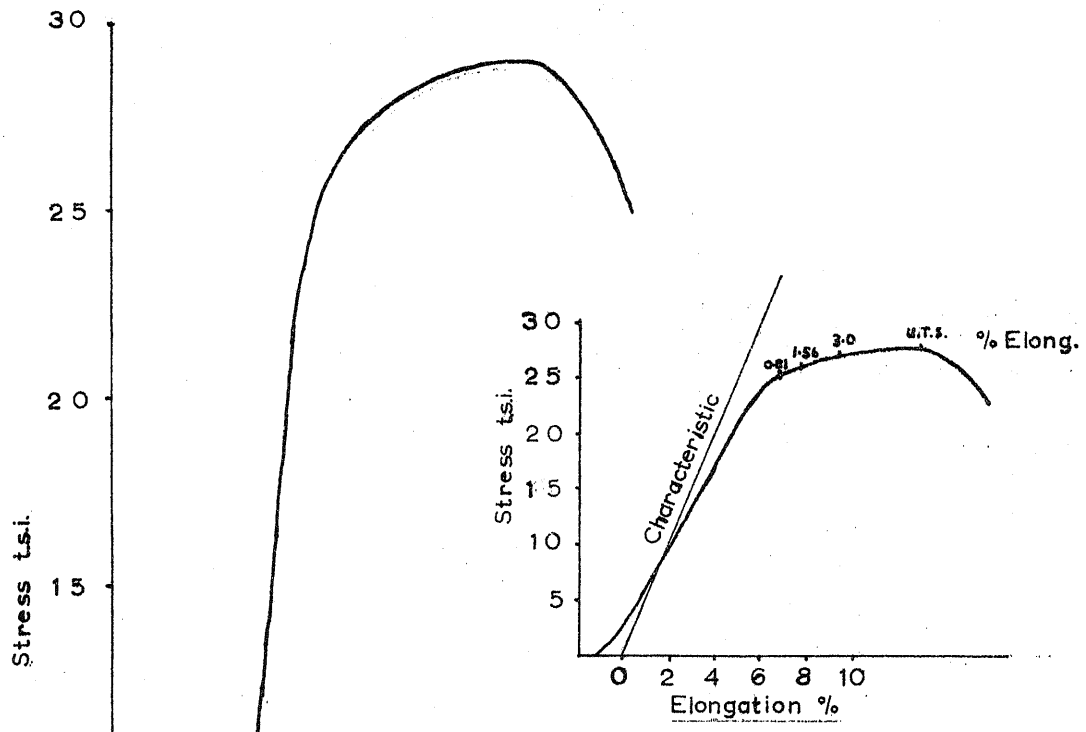

Figure 1

Tensile test of "heat treated" RR58. Strain rate 0.02/in.

D.F.L. 22.6 t.s.i.

U.T.S. 28.8 t.s.i.

$\frac{\text{D.P.L.}}{\text{U.T.S.}} = 0.784$

Elongation = 10.4%

Figure 2

Tensile test of "heat treated" RR58. Strain rate 0.05/in

D.F.L. = 21.2 t.s.i.

U.T.S. = 29.4 t.s.i.

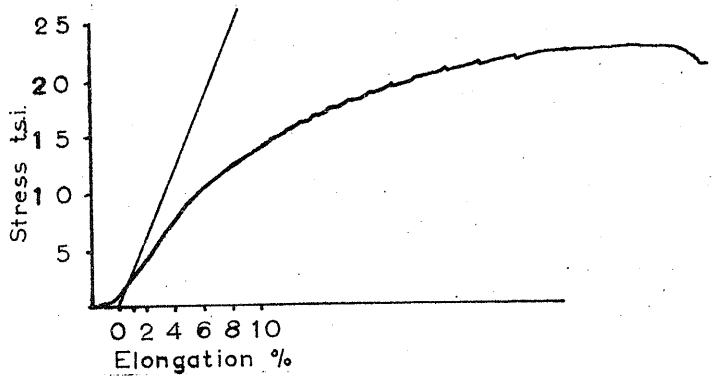

Figure 10

Tensile test of solution treated RR58.
Strain rate 0.027/in.

D.F.L. = 8.0 t.s.i.

U.T.S. = 19.5 t.s.i.

$\frac{\text{D.F.L.}}{\text{U.T.S.}}$ = 0.41

Elongation = 33%

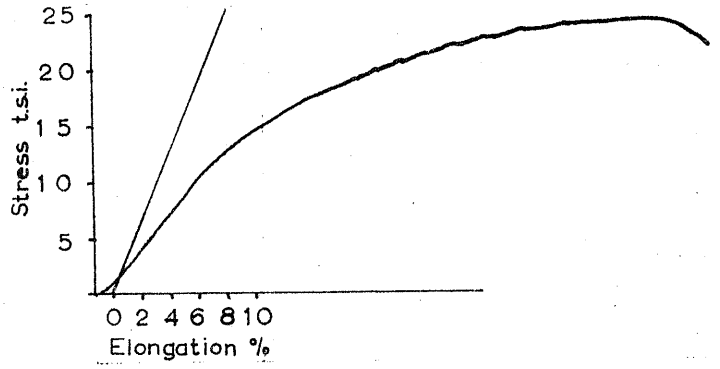

Figure 11

Tensile test of solution treated RR58.

Strain rate 0.0023/in.

D.F.L. = 9.5 t.s.i.

U.T.S. = 21.2 t.s.i.

$\frac{\text{D.F.L.}}{\text{U.T.S.}}$ = 0.45

Elongation = 31%

COLLEGE OF AERONAUTICS LIBRARY

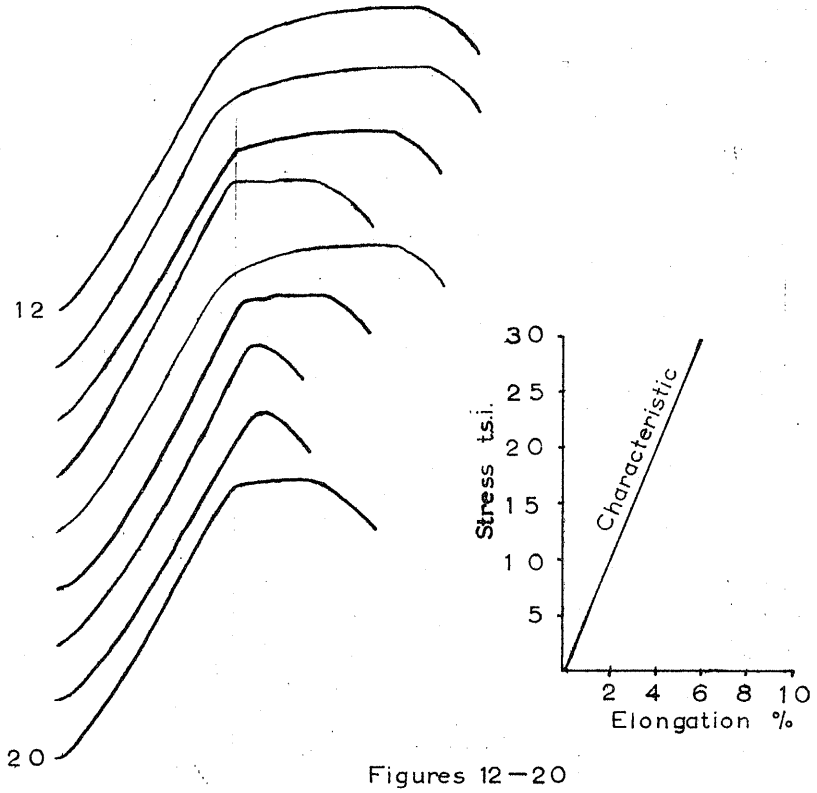

Figures 12—20

Tensile tests of "heat treated" RR58 specimens which have previously received cycling treatment

		Cycling treatment						Tensile test		
Fig. No.	Spec. No.	No. of cycles	Rest Period Time hrs.	Rest Period Temp. °C.	Max. stress t.s.i.	Min. stress t.s.i.	Original D.F.L.	D.F.L. t.s.i.	Y.P.	U.T.S. t.s.i.
12	7	100	4	20	22	20	-	23.2	-	28.6
13	8	100	4	20	24	22	-	22.2	-	28.5
14	9	100	4	20	26	24	-	24.3	26.0	27.7
15	10	100	4	20	28	26	-	26.4	28.1	28.1
16	13	None	-	-	-	-	-	20.0	-	26.4
17	24	100	4	20	26	24	-	25.3	26.5	27.0
18	27	100	5	20	27.9	25.8	-	27.0	27.3	27.8
19	28	1	5	20	27.1	-	-	23.8	26.2	26.2
20	32	1	5 mins	100	24.4	-	-	24.0	25.2	25.7

Rested 20 hours at $20^{\circ}C$

Figure 21

100 cycles
Max. stress 24.5 t.s.i.
Min. stress 20.5 t.s.i.

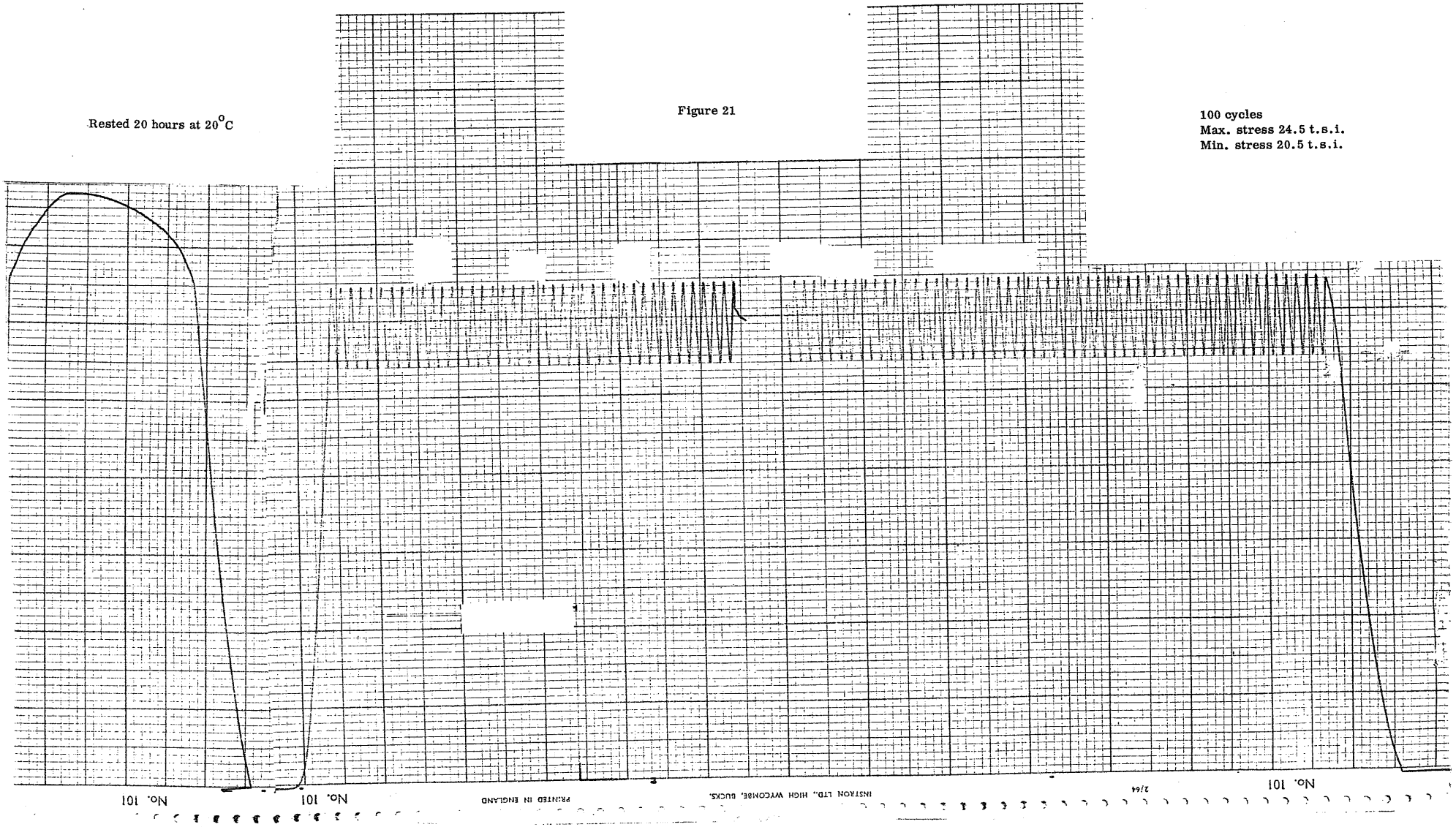

Figure 22

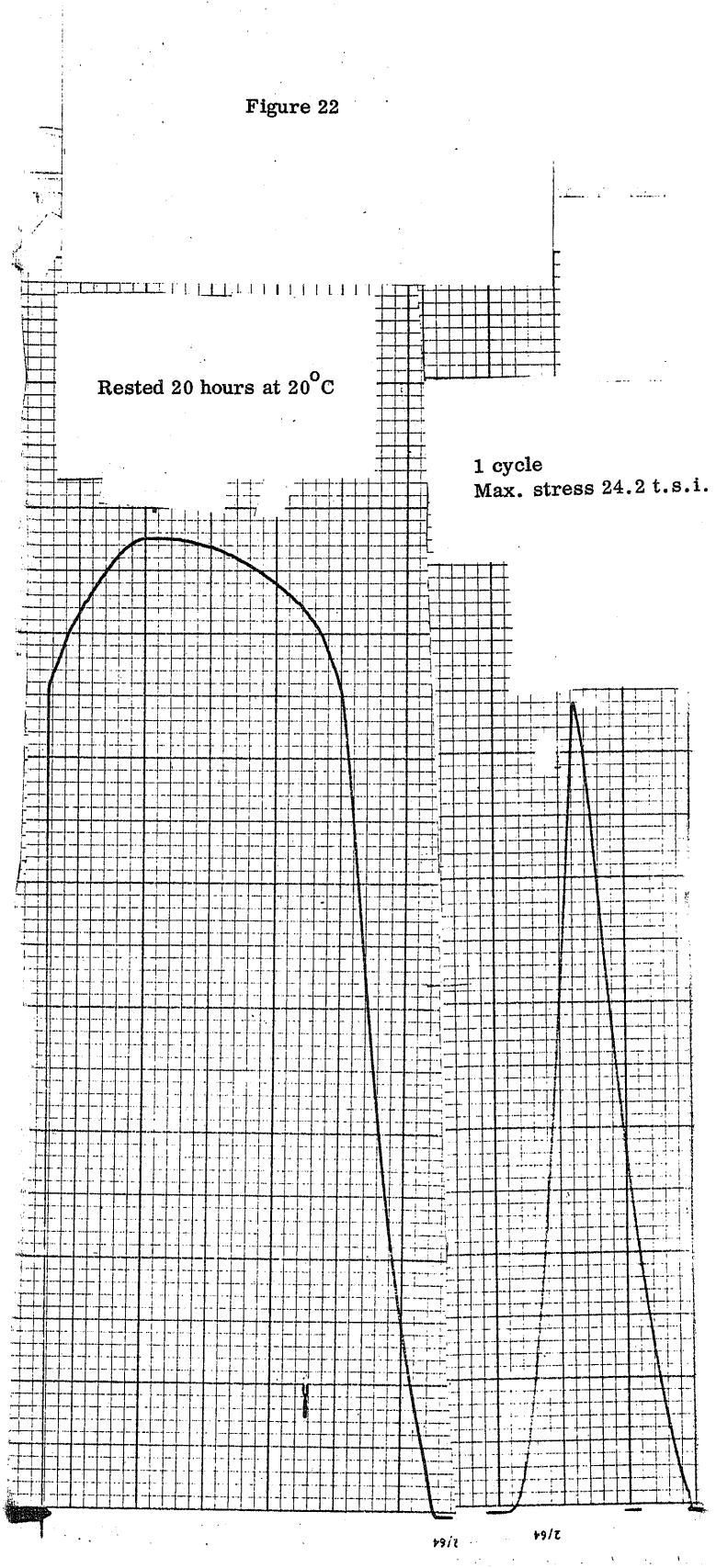

Figure 23

Rested 24 hours at 20^0C

100 cycles
Max. stress 26.3 t.s.i.
Min. stress 22.3 t.s.i.

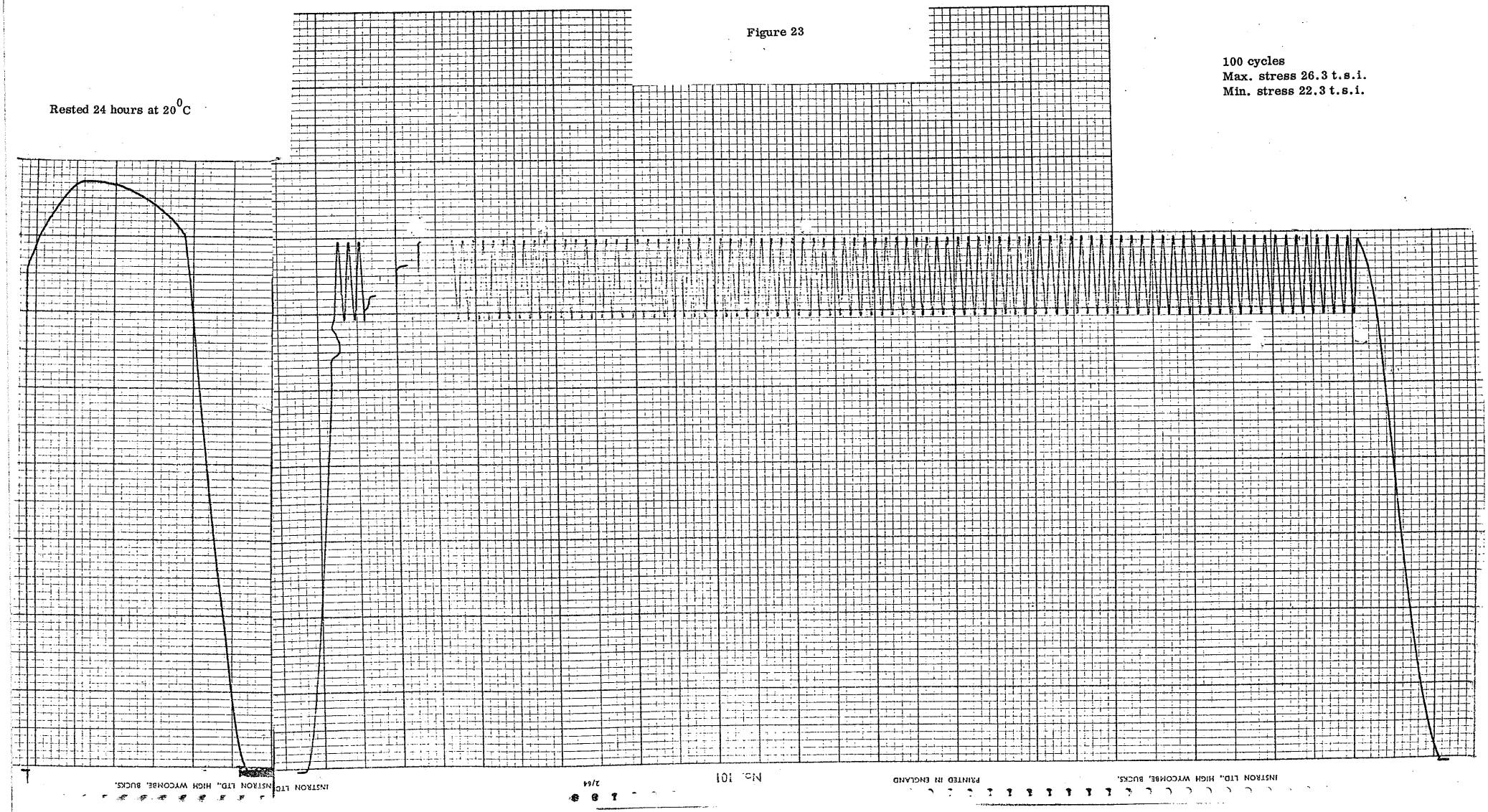

Figure 24

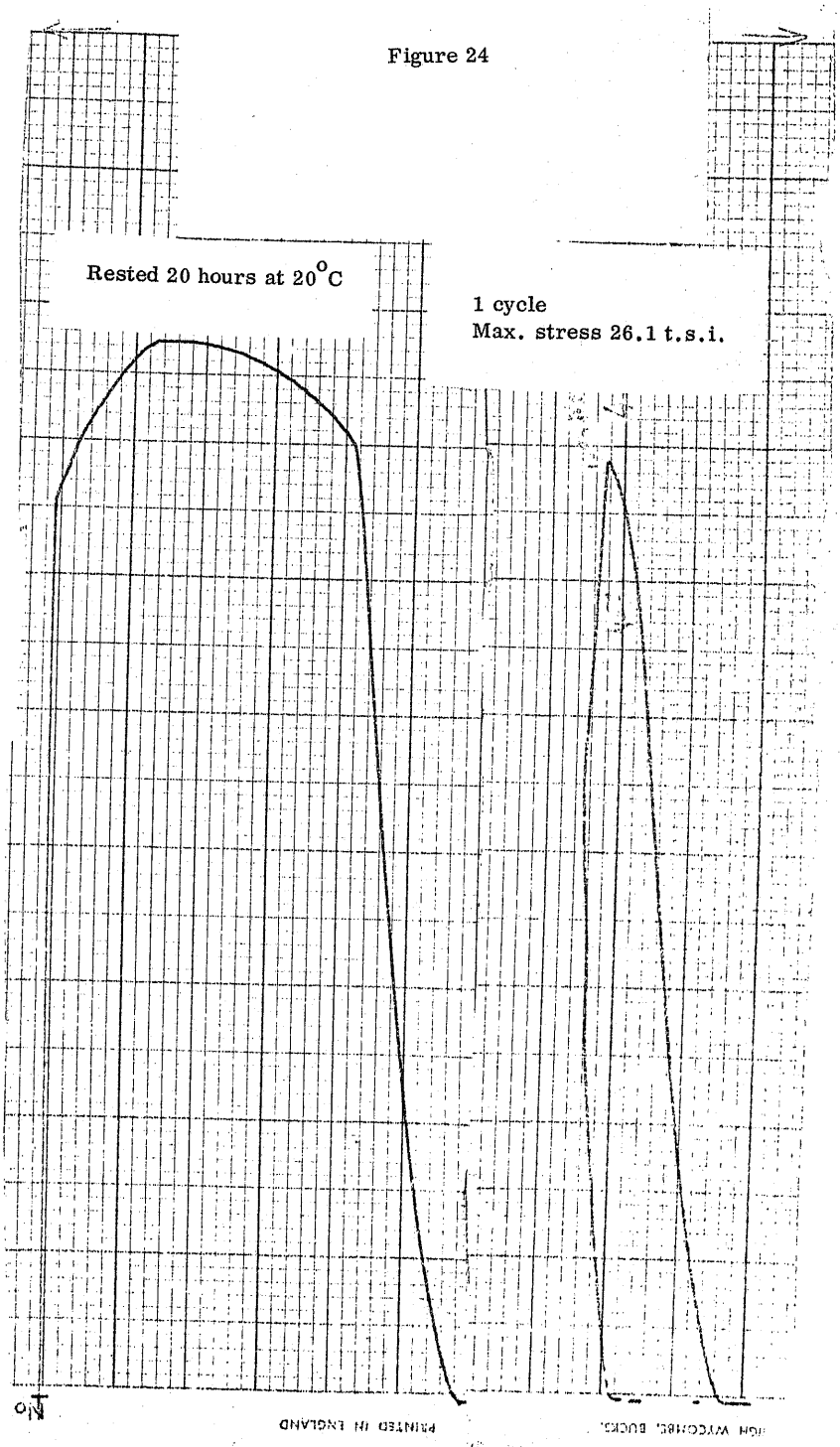

Figure 25

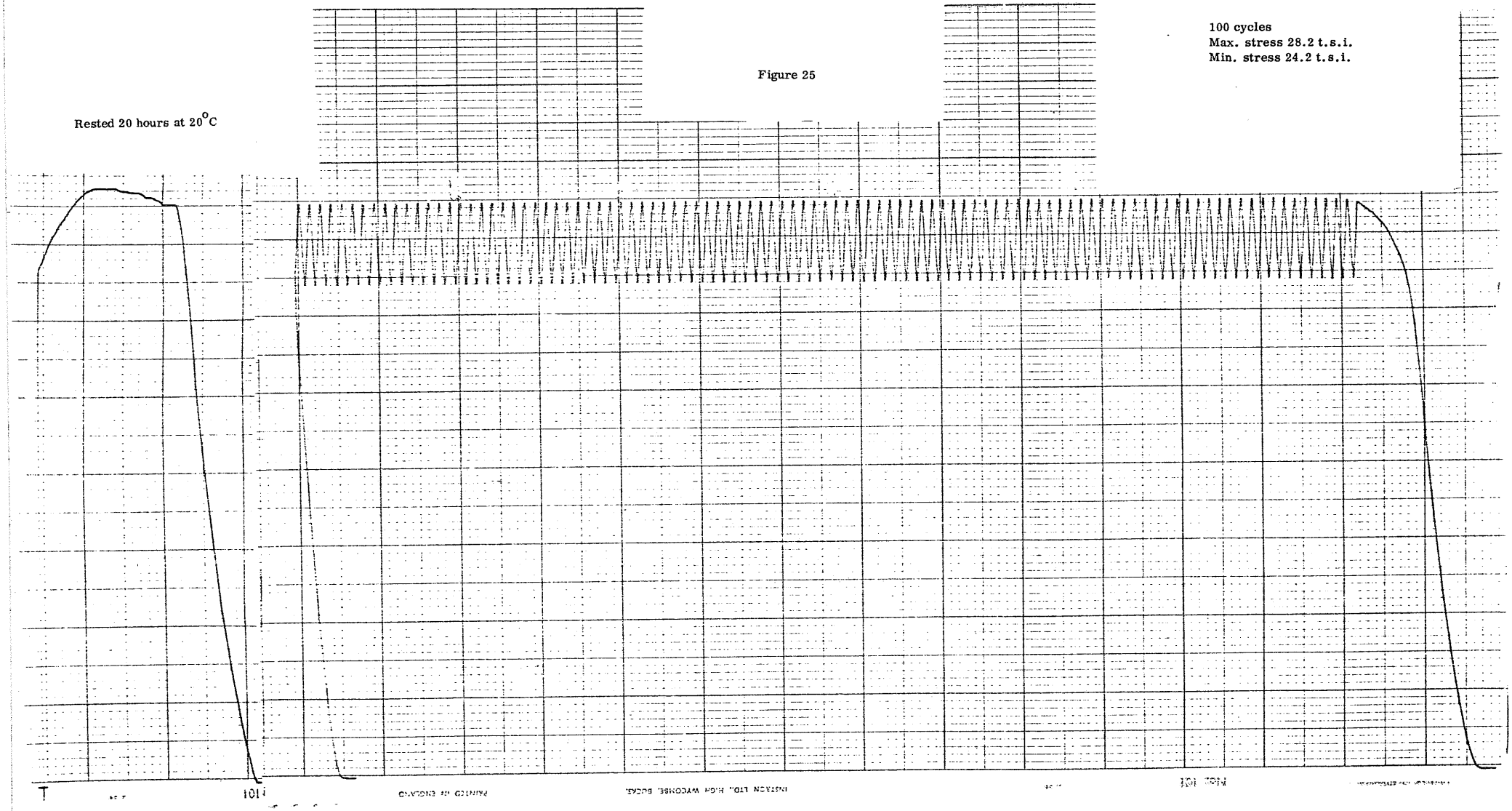
Rested 20 hours at 20°C
100 cycles
Max. stress 28.2 t.s.i.
Min. stress 24.2 t.s.i.

Figure 26

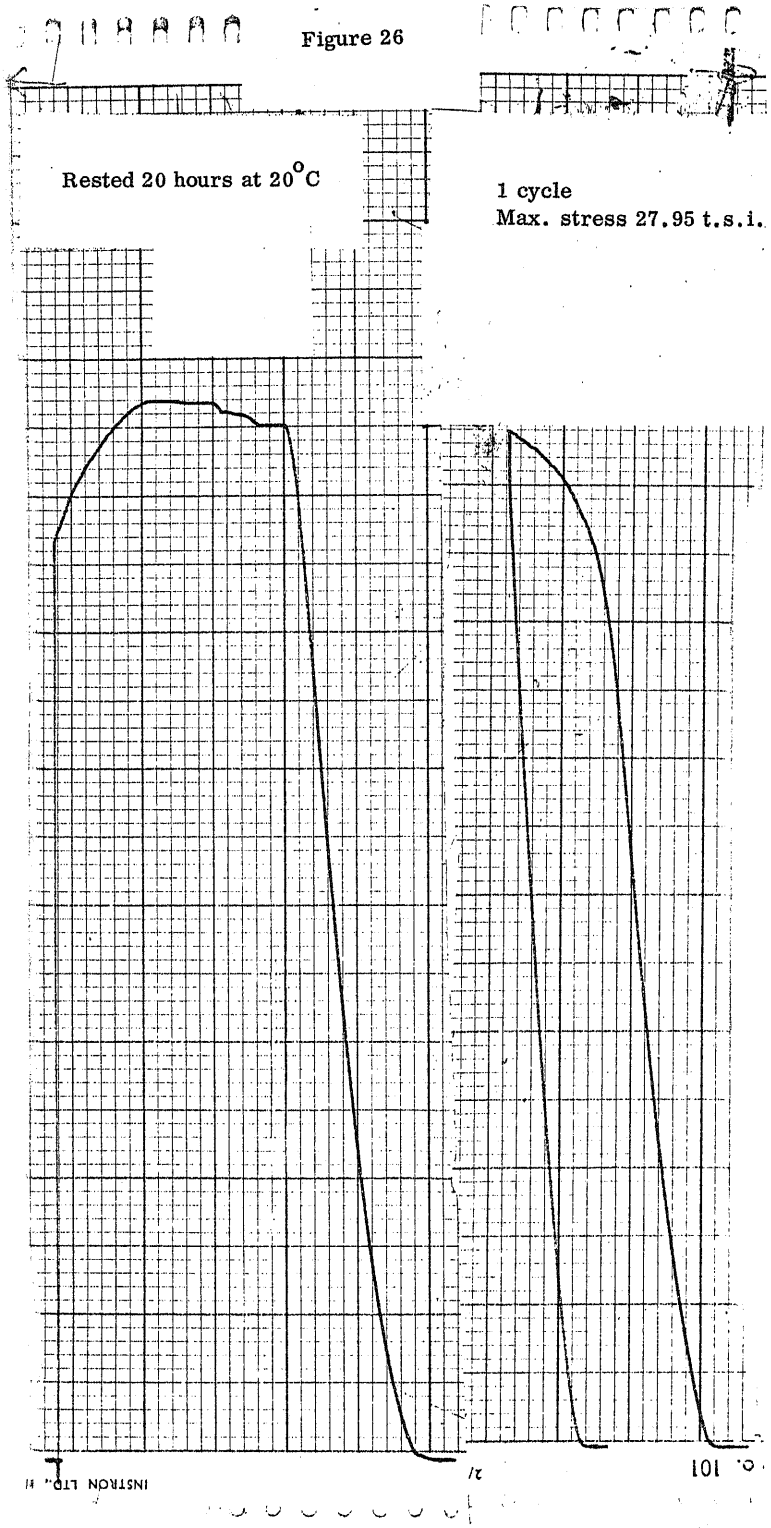

Tested immediately

Figure 27

100 cycles
Max. stress 28.2 t.s.i.
Min. stress 24.2 t.s.i.

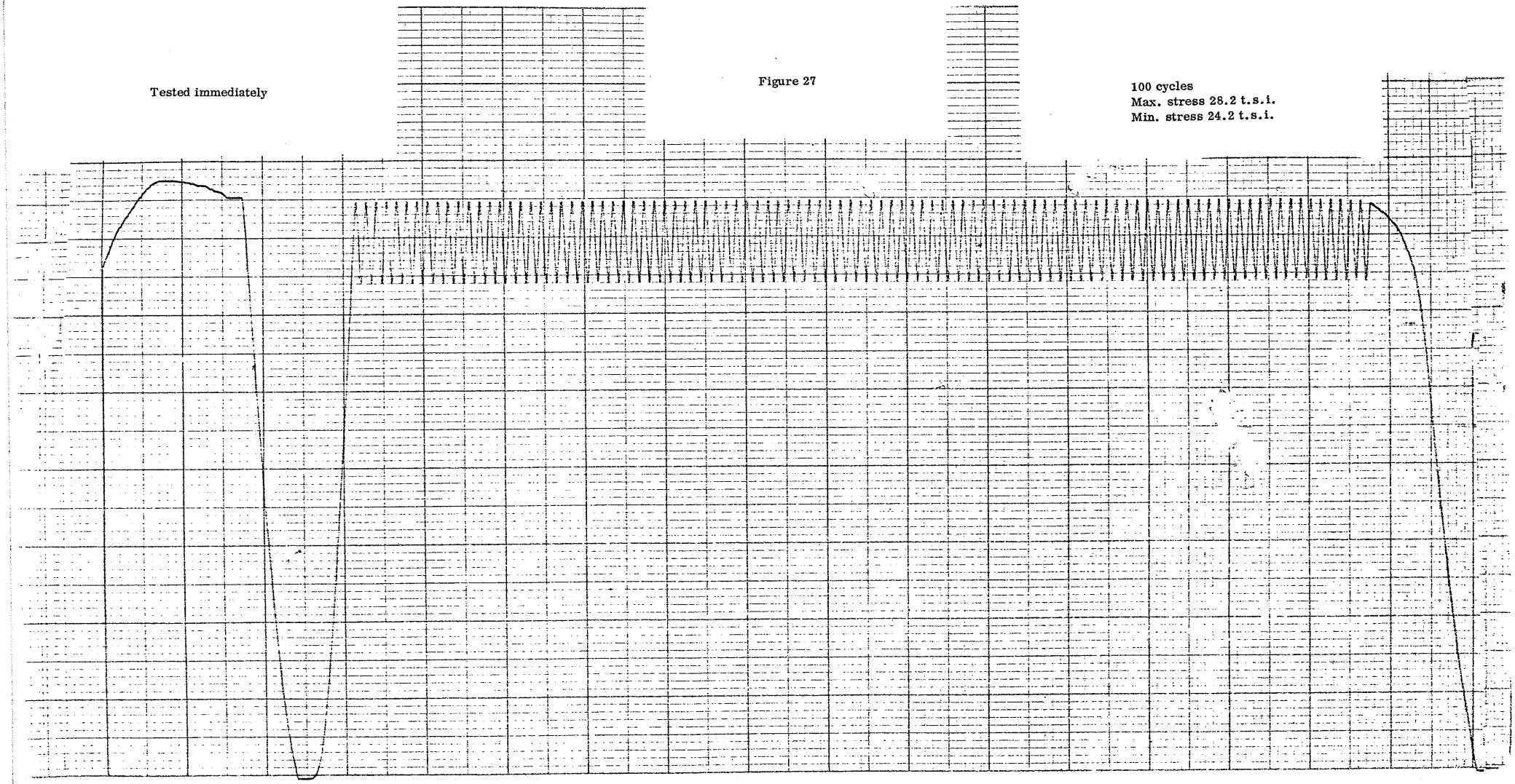

Figure 28

Tested immediately

1 cycle
Max. stress 28.2 t.s.i.

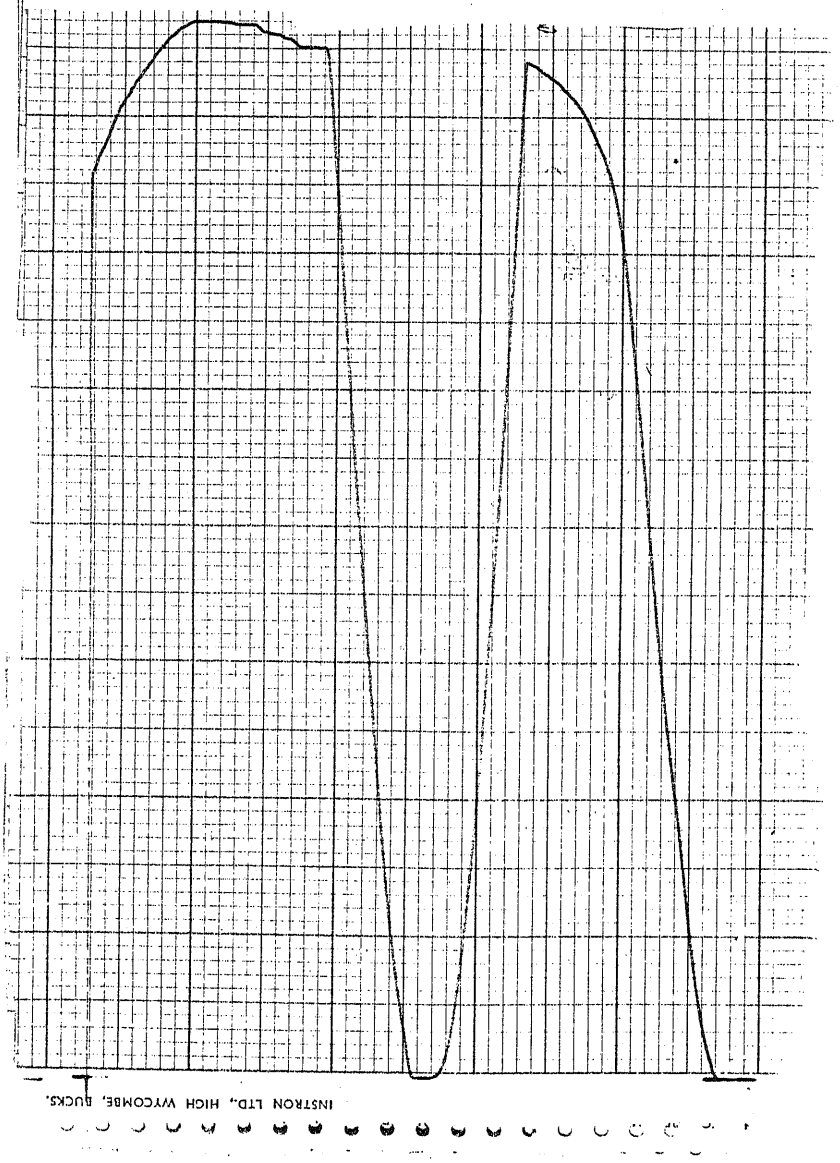

Figure 29

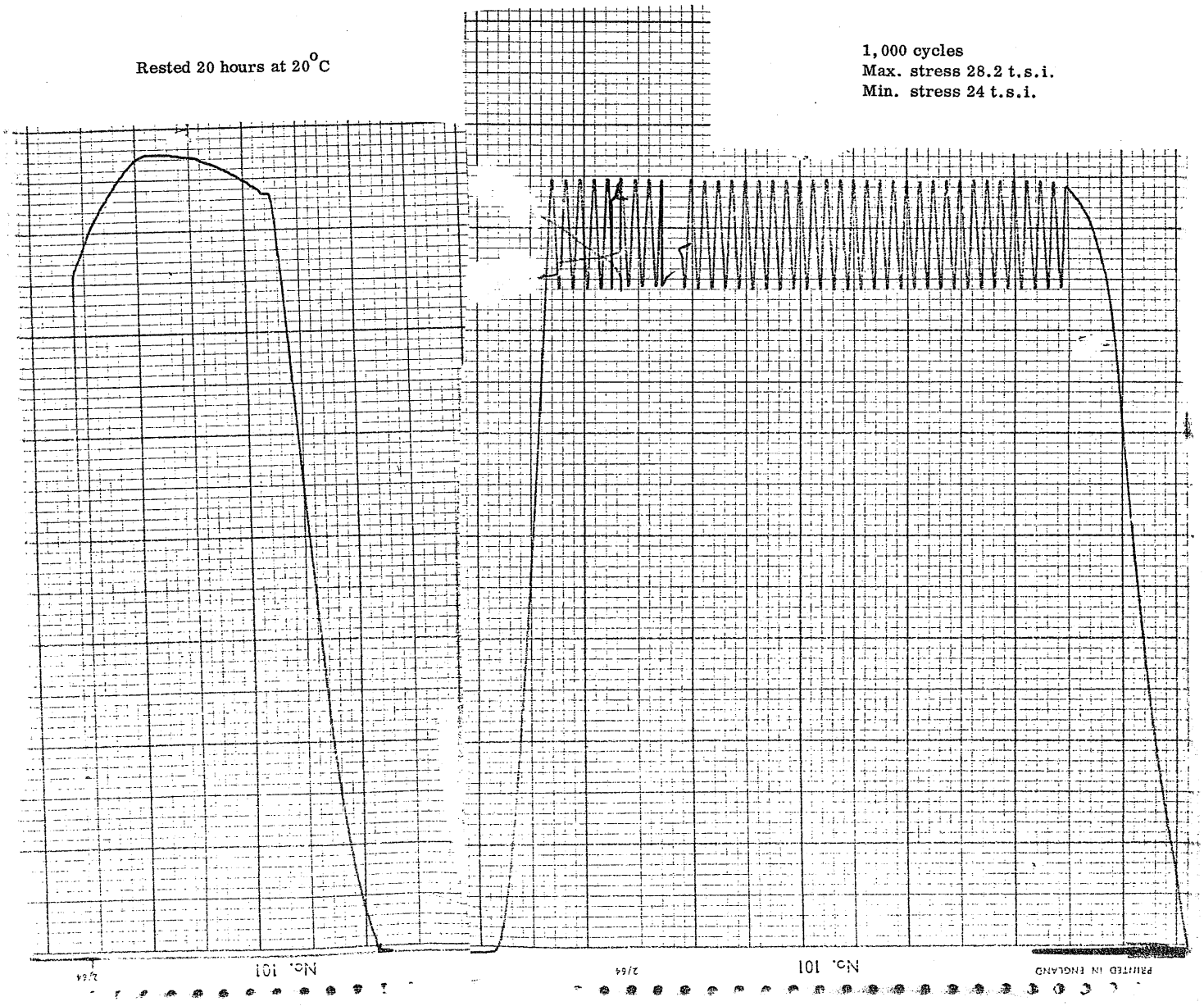
Rested 20 hours at 20°C
1,000 cycles
Max. stress 28.2 t.s.i.
Min. stress 24 t.s.i.
No. 101
2/64
No. 101
2/64
PRINTED IN ENGLAND

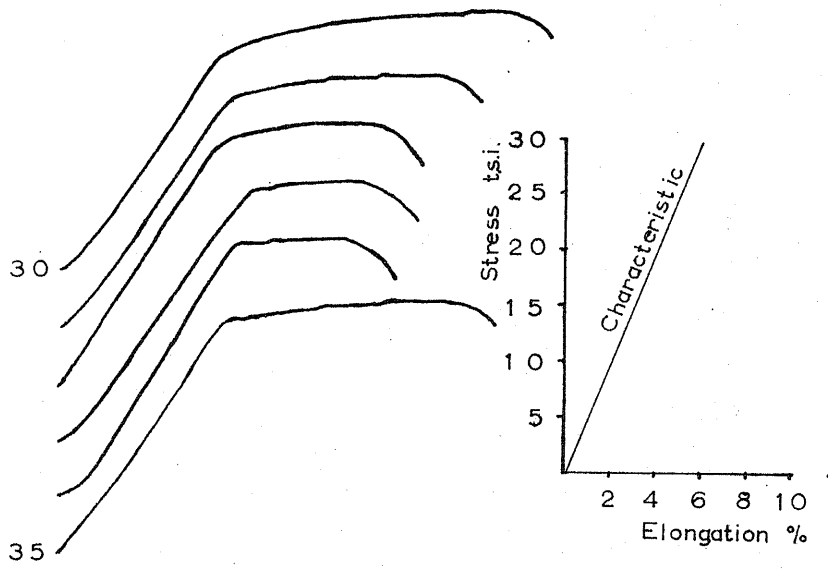

Figures 30 – 35

Tensile tests of "heat treated" RR58 subjected to 20 minute increments of creep and fatigue loading

Fig. No.	Static stress t.s.i.	Fatigue stress t.s.i.	Temp. °C.	D.F.L.	Y.P.	U.T.S.
30	17.2	± 0.25; 0.5; 1.0; 1.5; 2.0;	20	22.3	24.6	30.1
31	16; 18; 20; 22; 24; 26.	± 1.0	20	24.6	27.7	30.4
32	24	± 0.1; 0.5; 1.0; 1.5; 2.0; 2.5.	20	27.0	-	30.7
33	26	± 0.1; 0.5; 1.0; 1.5; 2.0; 2.5.	20	26.3	29.8	30.5
34	16; 18; 20; 22; 24; 26.	± 2.5	20	28.8	29.9	30.4
35	14.4; 16.4; 18.4; 20.4; 22.4; 24.4.	± 2.5	20	24.1	27.3	30.0

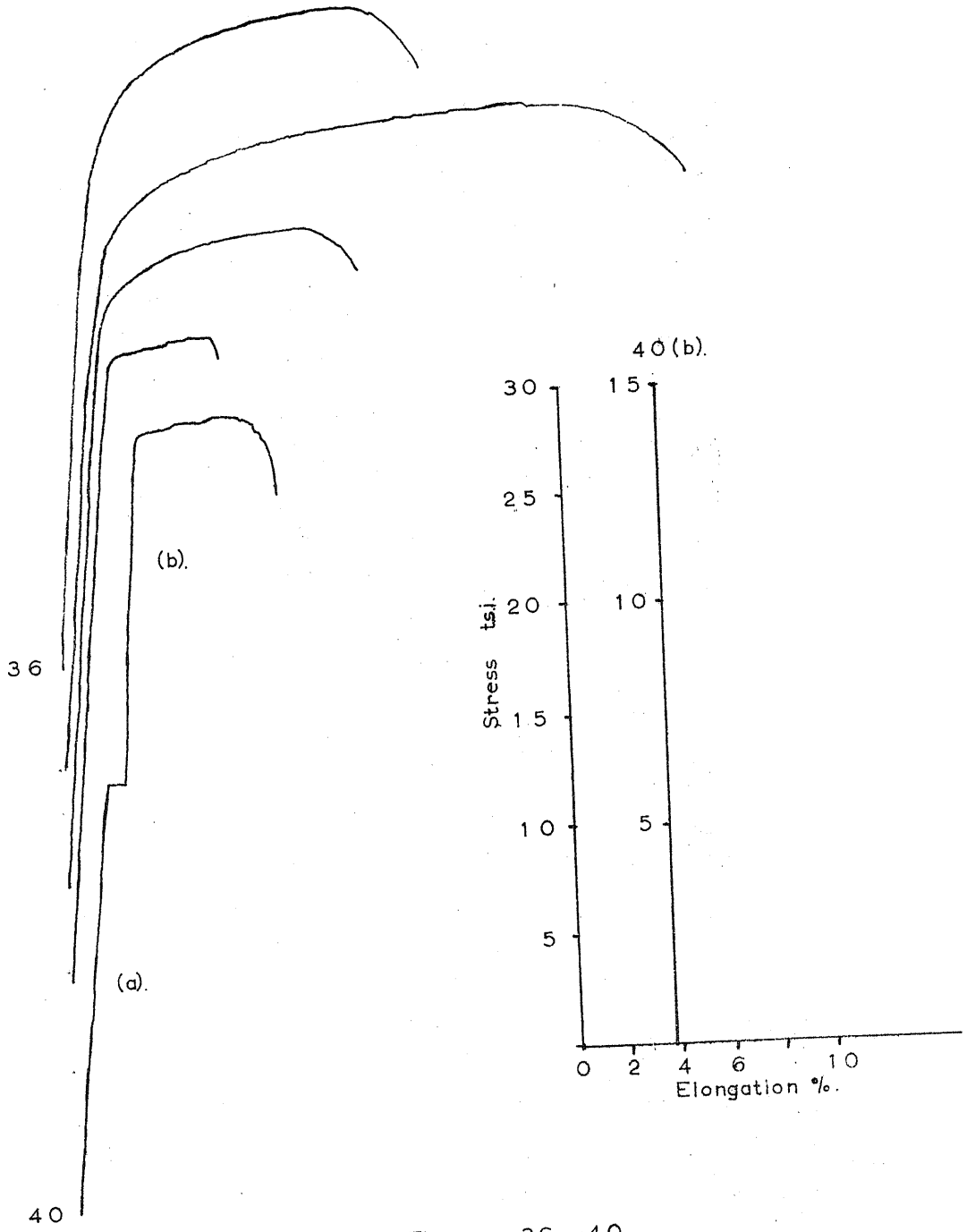

Figures 36—40

Tensile tests of "heat treated" RR58 subjected to 20 minute increments of creep and fatigue loading

Fig. No.	Static stress t.s.i.	Fatigue stress t.s.i.	Temp. °C.	D.F.L.	Y.P.	U.T.S.
36	14	± 0.1; 0.5; 1.0; 1.5; 2.0; 3.0.	130	18.5	-	29.6
37	18	± 0.1; 0.5; 1.0; 1.5; 2.0; 2.5	130	17.0	-	29.6
38	20	± 0.1; 1.0; 1.5; 2.0; 2.75.	130	22.7	-	29.5
39	22.3	± 0.1; 0.5; 1.0; 1.5; 2.0; 2.5.	130	25.2	-	29.3
40	16; 18; 20; 22; 24.	± 1.5	130	27.7	-	29.3

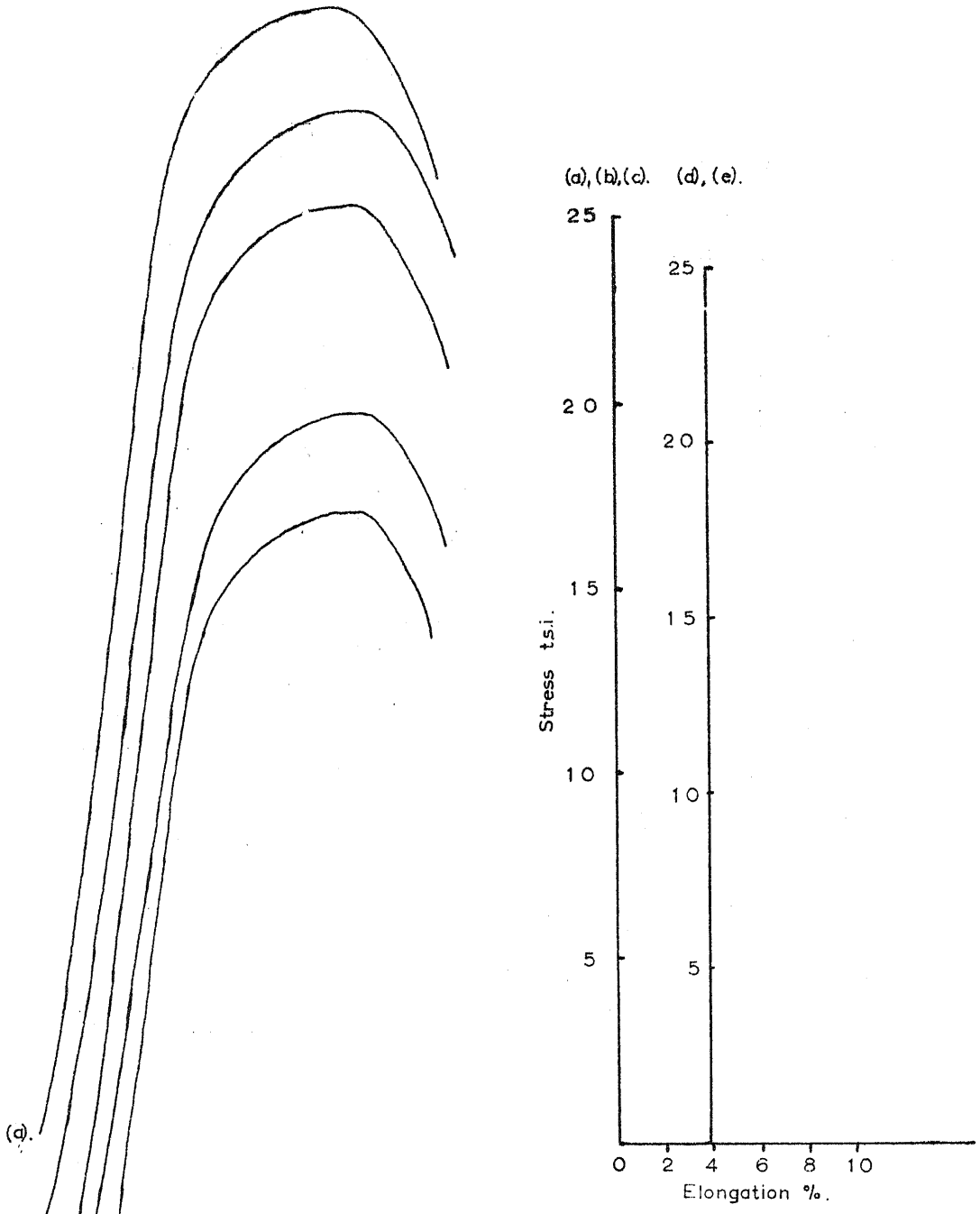

Tensile tests of fatigue specimens of heat treated RR58

Fig. No.	Max. stress	Min. stress	No. of cycles	D.F.L.	Y.P.	U.T.S.
41 (a)	+ 20 t.s.i.	- 20 t.s.i.	3,000	21.9 t.s.i.		29.6 t.s.i.
(b)	+ 10	- 10	60,000	21.5		29.8
(c)	+ 5	- 5	2.5×10^6	22.0		29.7
(d)	+ 22	+ 10	50,000	21.9		28.8
(e)	+ 22	0	50,000	21.6		29.5

Figure 41.

Part IV

Notes on some preliminary experiments on the combined creep and fatigue properties of RR58 over a range of temperatures at a frequency of 160 c/s

by

A. Younger, B.Sc., Ph.D., A.I.M.

Part IV

Introduction

In a previous section of this report (2.5) the desirability of combined creep and fatigue tests at frequencies greater than those obtainable on the hydraulic test machine was discussed. As a consequence of this need, a creep recording attachment was purchased for one of the Departmental 2-ton Amsler Vibrophore fatigue machines. This section reports the results of tests carried out with this equipment, repeating at 160 c/s many of the combinations of static loads, fatigue loads and temperatures used at the lower frequency. It was also possible with this equipment to increase the amplitude of the fatigue loading beyon that obtainable on the hydraulic test machine.

Experimental procedures

The tests were carried out on a standard 2-ton Amsler Vibrophore fatigue machine equipped with a load maintaining unit, a creep recorder and a furnace for elevated temperature tests. These three accessories are all standard attachments for the Vibrophore and are of Amsler manufacture.

The Vibrophore fatigue machine consists of an electromagnetic vibrator fitted to a cross-head sliding on two vertical pillars. The vertical position of the cross-head is fixed by a screw supporting the cross-head from a rigid beam connecting the upper ends of the two pillars. By rotation of the screw the cross-head may be raised or lowered to suit specimen length. It may also be used for applying a static load to the specimen. The vibrator is connected through a spring beam to the specimen, which at its lowered end is connected to a dynamometer. The deflection of the dynamometer is sensed optically and the amplitude of vibrations is controlled by photo-electric limiting devices operating on the deflection of the light beam. In tests where the fatigue amplitude mean is not zero, some creep will occur in the specimen. This creep results in a reduction in the static load. Consequently, a transducer mounted between the cross-head and the vibrator spring beam senses any reduction in load, and via a servo-motor readjusts the distance between the cross-head and the dynamometer by means of the loading screw. A mechanical device operated by the rotation of the servo-motor records on to a clockwork-driven chart the correction applied. This correction-time record is therefore a record of the creep extension of the specimen. Since, however, the transducer has to undergo a finite displacement before operating the servo-motor a stepped curve is produced. By arranging for the servo-motor to overshoot slightly, a regular hunting of the position of the cross-head may be

produced. This results in the smooth, but broad, curves seen in Figure 1. The width of the curve is a measure of the hunting amplitude, while the profile is a record of the creep behaviour. The hunting is, in fact, a superimposed secondary fatigue loading of frequency 1 c/s and maximum amplitude $\pm$ 4 lbs.

Adaptors manufactured for the Viborphore grips enabled identical specimens to those tested in the hydraulic machine to be used in these tests. The loading sequence followed the pattern described in Section 2, i.e. at a constant fatigue amplitude the static component was raised in 2 t.s.i. increments at time intervals of 20 minutes. The fatigue amplitudes selected were $\pm$ 2.5 t.s.i., $\pm$ 5 t.s.i., $\pm$ 7.5 t.s.i. With the $\pm$ 7.5 t.s.i. amplitude the initial static component was reduced to 12 t.s.i. to enable more than one combination to be achieved. With the two lower amplitudes a starting static load of 16 t.s.i. was used. The temperature range extended from 50 to 155^{o}C.

Results

The creep rates obtained with fatigue load of $\pm$ 2.5 t.s.i., $\pm$ 5.0 t.s.i. and $\pm$ 7.5. t.s.i. at 160 c/s over the temperature range 50 - 155^{o}C are given in Tables I - III. The creep rates, with applied fatigue loads of $\pm$ 2.5 t.s.i. and $\pm$ 5.0 t.s.i. increase with increasing static load, when this static load exceeds a certain value. This value appears to be 22 t.s.i. at 50^{o}C reducing to 20 t.s.i. at 155^{o}C for the $\pm$ 2.5 t.s.i. fatigue load and 20 t.s.i. at 50^{o}C reducing to 18 t.s.i. at 120^{o}C and above for the $\pm$ 5.0 t.s.i. fatigue. There is insufficient data to be sure of any trends under the $\pm$ 7.5 t.s.i. fatigue load.

Discussion

The limited results presented here are insufficient for detailed discussion. In particular, it is not possible to compare the creep rates at the same peak stress. Work is in progress to obtain this information.

However, it is possible to compare the creep rates obtained at the low (10 c/s) and high frequency (160 c/s) fatigue loads for the fatigue amplitude of $\pm$ 2.5 t.s.i. (Table IV). With only a very few exceptions the creep rate under 10 c/s fatigue is much faster than that under the higher frequency.

Temp. °C	Static Load 16	18	20	22	24	26	28
50	0.84	0.54	0.36	0	0.48	1.08	3.3
75	0	0.30	0.30	0	0.66	0.6	-
105	0	0.59	0.39	0.78	1.65	3.15	-
120	0	0.24	0.45	0.45	2.4	5.1	-
130	0	0.18	0.21	0.45	3.15	9.0	-
140	0.24	0.33	0.45	0.75	1.65	19.8	-
155	0.36	1.08	0.66	0.99	1.68	13.50	-

Table I. Creep at $\pm$ 2.5 t.s.i. fatigue at 160 c/s with increasing static loads. Units x 10^{-3} ins/in/hr.

Temp. °C	Static Load 16	18	20	22	24
50	0	0.24	0	0.69	0.90
75	0.45	0	0.21	1.32	3.30
105	0.84	0	0.48	1.20	21.0
120	0.24	0.90	1.65	12.0	-
130	0	0.66	1.95	6.30	-
140	0.12	0	0.75	26.40	-
150	0	0.54	6.30	-	-

Table II. Creep at $\pm$ 5.0 t.s.i. fatigue at 160 c/s with increasing static loads. Units x 10^{3} ins/ins/hr.

Temp.	Static Load			
°C	12	14	16	18
50			-0.3	0
75	-1.2	0	-0.12	1.95
105	-0.69	0.36	0.21	
120	-0.39	-0.51	0.45	3.3
130	0	0.36		
140	0	0.27	1.2	9.6
155			0	

Table III. Creep at $\pm$ 7.5 t.s.i. fatigue at 160 c/s with increasing static loads. Units x 10^3 ins/ins/hr.

Temp.		Static Load t.s.i.					
°C		16	18	20	22	24	26
50	a.	0.84	0.54	0.36	0	0.48	1.08
	b.	0	1.8	0	1.2	6.0	4.5
75	a.	0	0.30	0.30	0	0.66	0.6
	b.	1.1	0.9	0	0.9	2.1	-
105	a.	0	0.59	0.39	0.78	1.65	3.15
	b.	0	0.9	0	3.0	27.0	-
120	a.	0	0.24	0.45	0.45	2.4	5.1
	b.	1.2	1.0	0	12.0	45.0	-
130	a.	0	0.18	0.21	0.45	3.15	9.0
	b.	0	0	1.3	11.1	-	-
140	a.	0.24	0.33	0.45	0.75	1.65	19.8
	b.	0	0	3.0	129	-	-
155	a.	0.36	1.08	0.66	0.99	1.68	13.5
	b.	0.9	0	4.2	468	-	-

a. fatigue at 160 c/s
b. fatigue at 10 c/s

Table IV. Comparison of creep rates at two fatigue frequencies of constant amplitude $\pm$ 2.5 t.s.i. over a range of temperatures and static loads.

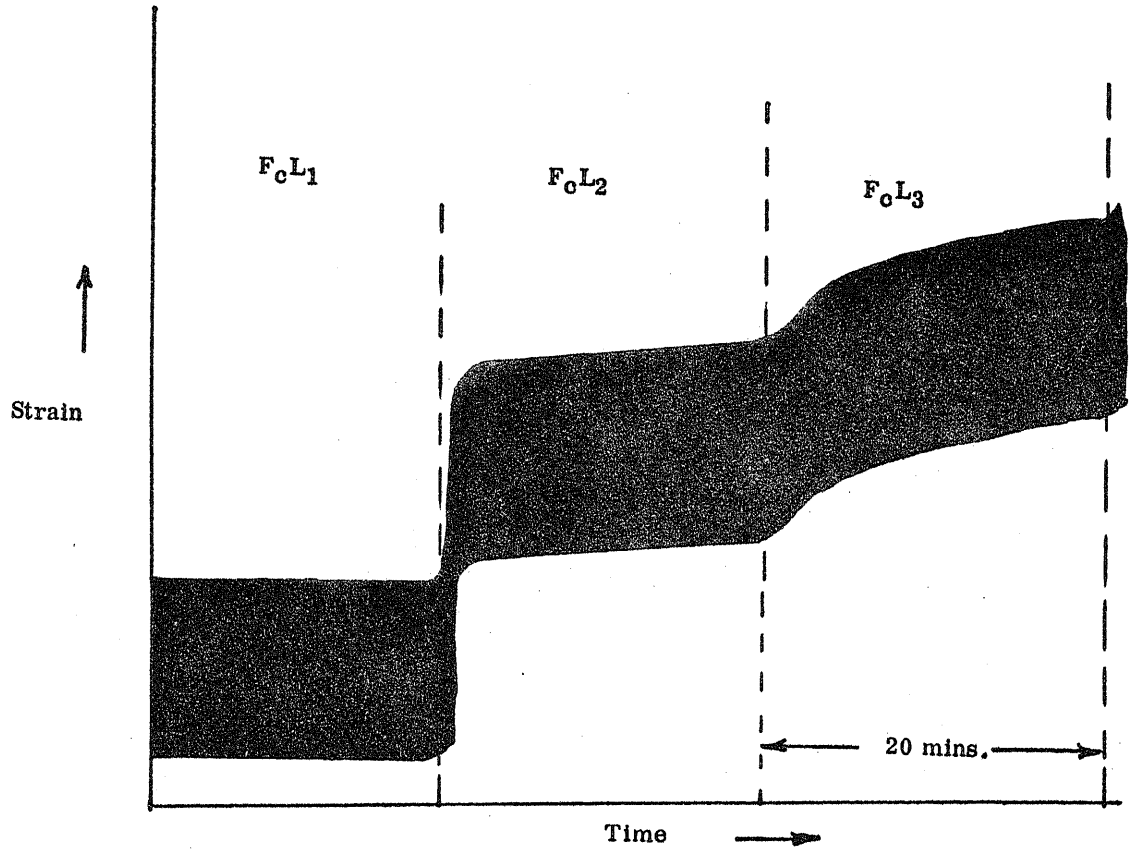

Figure 1 Typical strain-time record